Turkish Journal of Earth Sciences (Turkish J. Earth Sci.), **Vol. 17**, 2008, pp. 85–109. *Copyright ©TÜBİTAK*
First published online 21 November 2007

Petrology and ^{40}Ar-^{39}Ar Age of the Bimodal Orduzu Volcanics (Malatya) from the Western end of the Eastern Anatolian Neogene Volcanism, Turkey

AYTEN ÖNAL[1], DURMUŞ BOZTUĞ[2], MEHMET ARSLAN[3],
TERRY L. SPELL[4] & SEVCAN KÜRÜM[5]

[1] Department of Mining Engineering, İnönü University, TR–44280 Malatya, Turkey
[2] Department of Geological Engineering, Cumhuriyet University, TR–58140 Sivas, Turkey
(E-mail: durmus.boztug@gmail.com)
[3] Department of Geological Engineering, Karadeniz Technical University, TR–61080 Trabzon, Turkey
[4] Department of Geosciences, University of Nevada, Las Vegas, Nevada 89154, USA
[5] Department of Geological Engineering, Fırat University, TR–23119 Elazığ, Turkey

Abstract: The Orduzu volcanics, which are part of the Yamadağ volcanics in the Malatya region, include rhyolite, rhyolitic dykes, trachyandesite and basaltic trachyandesitic dykes. Mafic globular occurrences within the basaltic trachyandesitic dykes, the existence of basaltic trachyandesite enclaves within the trachyandesite, and other textural and geochemical evidence all indicate magma mingling/mixing. Incremental ^{40}Ar-^{39}Ar dating on plagioclase from the rhyolite, from rhyolite dykes and basaltic trachyandesite yielded consistently 16 Ma (Middle Miocene). Primordial mantle-normalized spider diagrams of the rhyolite and rhyolitic dykes represent enrichments in some large ion lithophile elements (Cs, Rb, Ba, K, Th, U) but remarkably depletion in Sr, Nb, Ti, Eu and slight depletion in some high field strength elements (Hf, Zr) relative to the trachyandesites and basaltic trachyandesitic dykes. Chondrite-normalized rare earth element spidergrams yield a high $(La/Lu)_{CN}$ (18–47) and Eu/Eu* (0.57–0.92) ratios for the rhyolites and rhyloitic dykes, but a low $(La/Lu)_{CN}$ (7–13) and Eu/Eu* (0.86–1.05) values for the trachyandesites and basaltic trachyandesitic dykes. From the field relations and geochemical data, it is concluded that three distinct magma sources were spatially and temporally involved in the genesis of the Orduzu volcanics, that include a calc-alkaline, crustal-derived rhyolitic melt, another calc-alkaline, lithospheric mantle-derived andesitic magma, and a mildly alkaline, lithospheric mantle-derived basaltic magma.

Key Words: petrology, Ar-Ar dating, Neogene volcanism, Malatya, Eastern Anatolia, Turkey

Doğu Anadolu Neojen Volkanizmasının Batısındaki Bimodal Orduzu (Malatya) Volkanitlerinin Petrolojisi ve ^{40}Ar-^{39}Ar Yaşı

Özet: Doğu Anadolu'da yaygın olarak yüzeylenen Neojen magmatizmasının bir ürünü olan Yamadağ volkanitlerine ait Orduzu volkanitleri (Malatya), riyolit, riyolitik dayk, trakiandezit ve bazaltik trakiandezit dayklarından oluşmaktadır. Bazaltik trakiandezitik dayklardaki mafik globüller, trakiandezitiklerdeki bazaltik trakiandezit anklavları, bazı mikroskopik dokusal özellikler ve jeokimyasal bulgular magma karışmasının verileri olarak değerlendirilmiştir. Orduzu volkaniti kayaçlarında aşamalı gazsızlaştırma tekniğiyle yürütülen ^{40}Ar-^{39}Ar radyometrik yaş tayini çalışmalarında, riyolitlerde, riyolitik dayklarda ve bazaltik trakiandezitik dayklarda Orta Miyosene karşılık gelen yaşlar (16 My) elde edilmiştir. Primordial manto'ya göre normalleştirilmiş örümcek diyagramları, riyolit ve riyolitik daykların, andezit ve bazaltik trakiandezitik dayklara göre bazı büyük iyon çaplı elementler (Cs, Rb, Ba, K, Th, U) bakımından zenginleşme; ancak Sr, Nb, Ti bakımından kuvvetli ve bazı kalıcılığı yüksek elementler (Hf, Zr) bakımından ise hafifçe fakirleşmeye uğradıklarını göstermektedir. Chondrit'e göre normalleştirilmiş nadir toprak elementleri örümcek diyagramları ise riyolit ve riyolitik dayklar için bağıl olarak nisbeten daha yüksek bir $(La/Lu)_{CN}$ (18–47) ve Eu/Eu* (0.57–0.92) oranları; trakiandezitler ve bazaltik trakiandezitik dayklar için ise daha düşük bir $(La/Lu)_{CN}$ (7–13) ve Eu/Eu* (0.86–1.05) oranları gösterirler. Jeokronolojik, arazi, petrografik ve jeokimyasal veriler, Orduzu volkanitlerinin oluşumunda, konumsal ve zamansal olarak üç farklı magmanın etkin olduğunu göstermektedir. Bunlar, (1) kabuksal kökenli, kalk-alkalen riyolitik magma; (2) litosferik manto kökenli, kalk-alkalen magma; (3) litosferik manto kökenli orta derece alkalen magma kaynağıdır.

Anahtar Sözcükler: petroloji, argon-argon yaş tayini, Neojen volkanizması, Malatya, Doğu Anadolu, Türkiye

Introduction

Miocene to Quaternary volcanism in east and southeast Turkey has been intensively studied by numerous authors (e.g., Leo *et al*. 1974; Innocenti *et al*. 1982; Pearce *et al*. 1990; Yılmaz 1990; Keskin *et al*. 1998; Yalçın *et al*. 1998; Arger *et al*. 2000; Keskin 2003; Alpaslan *et al*. 2004; Kürüm *et al*. 2004; Ekici *et al*. 2006; Özdemir *et al*. 2006). Their interpretations largely suggest that this volcanism is related to the ongoing convergence between the Arabian and Eurasian plates. Keskin (2003) and Keskin *et al*. (2006) summarized the genetic models suggested by various authors for the eastern and southeastern Anatolian volcanics as follows: (1) the tectonic escape of micro-plates to the east and west, (2) the subduction of the Arabian plate beneath eastern Anatolia, (3) the melting of normal asthenosphere by adiabatic decompression of upwelling mantle resulting from extension, (4) continental collision and subsequent thickening of the Anatolian lithosphere, (5) the delamination of mantle lithosphere beneath the region. Keskin (2003) reported that all these mechanisms, proposed before 2000, are not consistent with recent geophysical research indicating the absence of mantle lithosphere beneath eastern Anatolia (Şengör *et al*. 2003). Based on these new geophysical results, Keskin (2003) and Şengör *et al*. (2003) proposed that the slab break-off mechanism resulted from continuing compression between the Eurasian and Arabian plates around 13 Ma, and may be responsible for widespread Miocene and younger volcanics in east Anatolia.

The volcanic rocks, covering a vast area (ca. 1500 km^2) between Sivas in the north and Kahramanmaraş in the south, constitute the western part of the east Anatolian Neogene volcanism (Figure 1a, b), and yield Middle to Late Miocene radiometric ages (Leo *et al*. 1974; Arger *et al*. 2000; Kürüm *et al*. 2004). Volcanics in the northern part of this province, exposed across a wide area between Sivas to the northwest and Malatya to the southeast, and including the Orduzu-Malatya region, are known as the Yamadağ volcanics (S. Yılmaz *et al*. 1993; Yalçın *et al*. 1998; Kürüm *et al*. 2004; Figure 1). The Yamadağ volcanics constitute a vast volcanic sequence which from bottom to top mainly comprises rhyolitic lavas, andesitic lava and pyroclastic intercalations, and basaltic/andesitic to andesitic/dacitic lava flows (Yalçın *et al*. 1998; Kürüm *et al*. 2004).

This paper deals mainly with the mineralogy-petrography, ^{40}Ar-^{39}Ar age determination and geochemistry of the Orduzu volcanics (Malatya), which form the western end of the Neogene volcanism in eastern Anatolia, Turkey, in order to bring some new solid contribution to the local geology and to understand better the geological evolution of Eastern Anatolian Neogene volcanism.

Geological Setting & Field Relations

Recent studies show that the Neogene volcanism in eastern Anatolia can be classified into three stages with respect to age and geodynamic setting, as follows: (1) syn-collisional Oligocene–Early Miocene felsic volcanism associated with the collision of Eurasia and Arabia (e.g., H. Yılmaz *et al*. 2007); (2) Middle Miocene felsic volcanism generated in a post-collisional extensional setting (e.g., Kürüm *et al*. 2004; H. Yılmaz *et al*. 2007) and (3) Late Miocene to Plio–Quaternary volcanism generated in a post-collisional setting related to either lithospheric detachment (e.g., Pearce *et al*. 1990) or slab break-off (e.g., Keskin 2003; Şengör *et al*. 2003; Keskin *et al*. 2006).

The Orduzu volcanics are a part of the widespread Middle to Late Miocene Yamadağ volcanics (Yalçın *et al*. 1998; Kürüm *et al*. 2004) in Malatya province, which form the western part of the Neogene volcanism in eastern Anatolia (Figure 1). Forming the basement of the Orduzu volcanics are Middle Eocene fossiliferous flysch rock associations (Demir 1997; Figures 2 & 3). The Orduzu volcanics comprise rhyolite, rhyolitic dikes, trachyandesite and basaltic trachyandesitic dikes, and the rhyolite is exposed clearly cutting the Middle Eocene flysch (Figures 2 & 3). Quaternary unconsolidated gravels and sands unconformably overlie all these rocks. The field relations between the Orduzu volcanics and country rocks may indicate a volcanic centre. Futhermore the field relations of rhyolitic and basaltic trachyandesitic dykes reveal a ring dyke structure.

The rhyolites constitute the first lava flows in the volcanic sequence (Figures 2, 3 & 4a) and are cut by rhyolitic ring dykes (Figure 4b). The thickness of these ring dykes varies from 30 to 125 m, and the thickest dyke may also have been a feeder dyke. The trachyandesite is younger than the rhyolites and rhyolitic dykes, since it apparently overlies them (Figures 2, 3 & 4c).

The trachyandesite locally includes ovoid, fine-grained (Ø ~1–2 mm) basaltic trachyandesite enclaves ranging

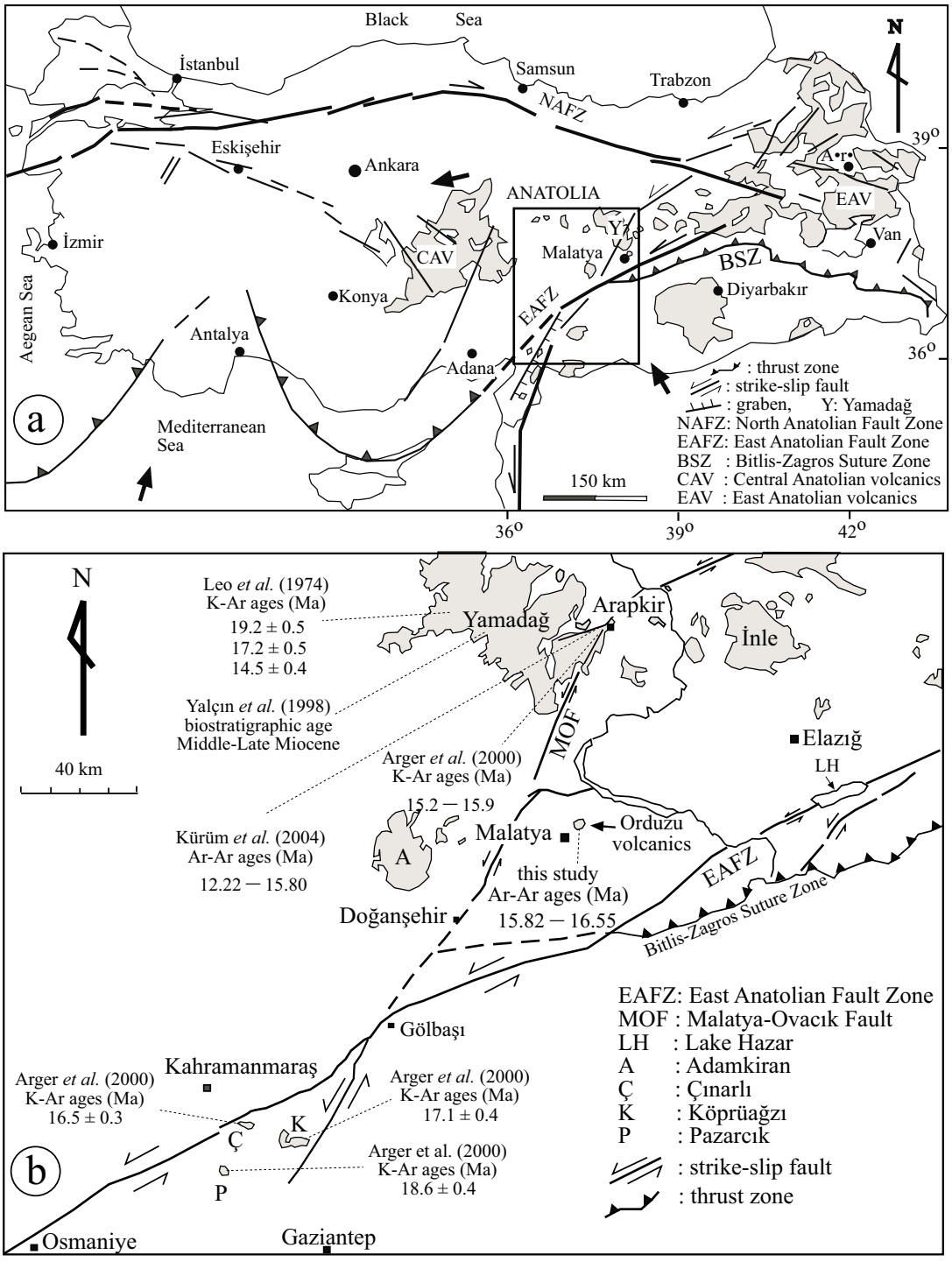

Figure 1. (a) Location map of volcanic rocks from Miocene to Quaternary in central and east Anatolia (simplified after Temel *et al.* 1998); (b) location map of Neogene volcanics in Kahramanmaraş-Malatya-Elazığ region (simplified Arger *et al.* 2000).

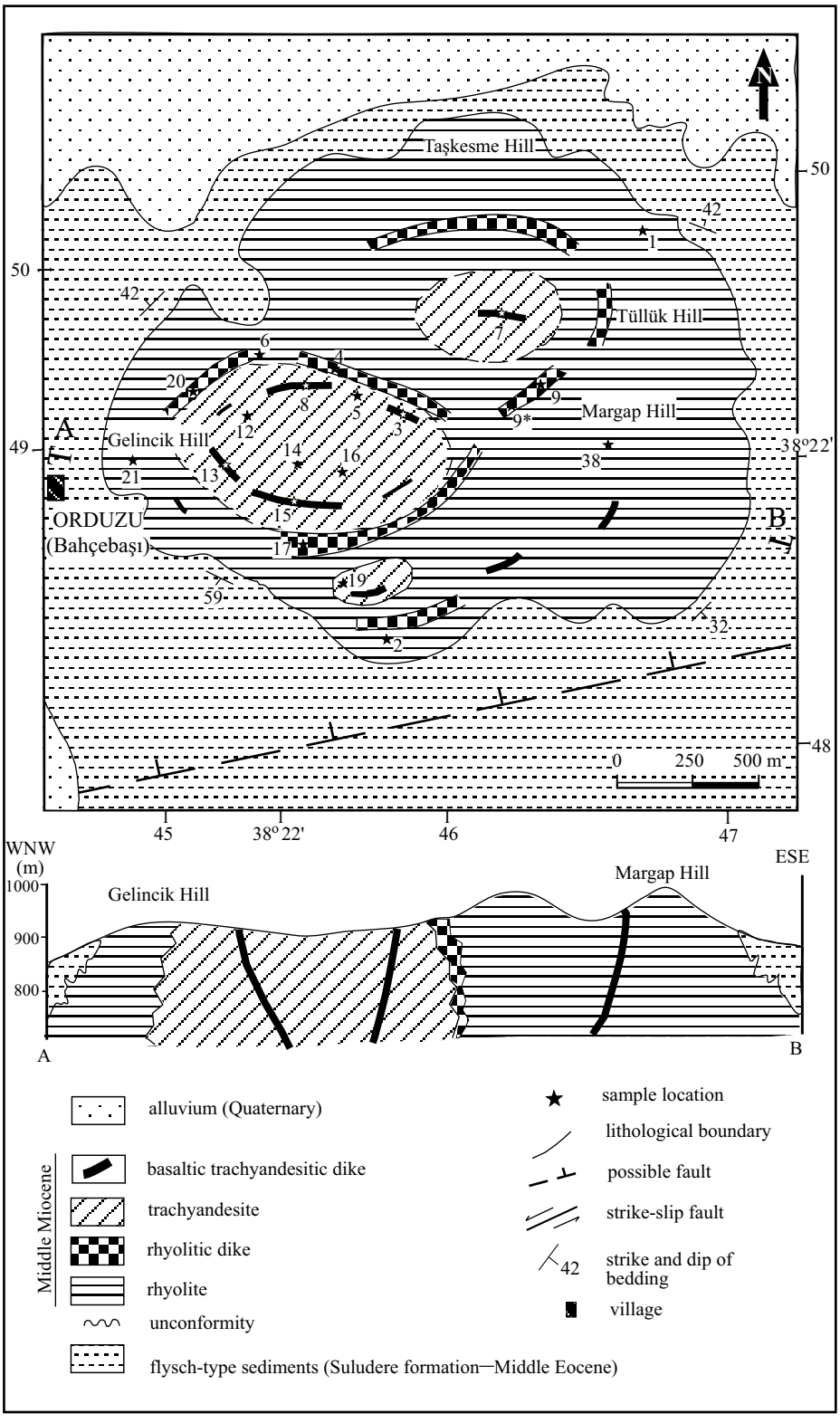

Figure 2. Geological map and cross-section of the Orduzu volcanics.

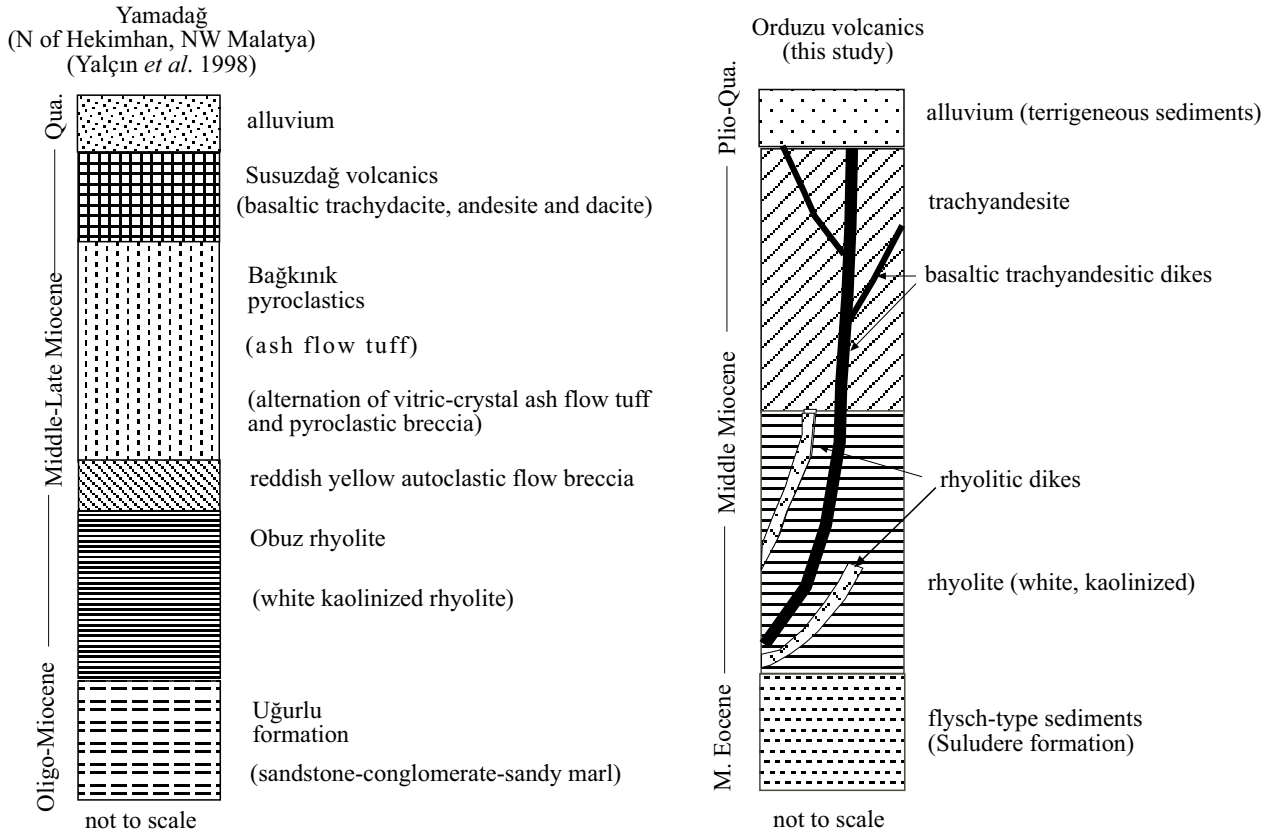

Figure 3. Stratigraphic setting of the Orduzu volcanics in the generalized columnar section of the widespread Yamadağ volcanic rocks.

from 3 to 30 cm in diameter (Figure 4d). These ovoid, less deformed and small enclaves may be products of the mingling process between coeval trachyandesitic and basaltic magmas within the volcanic conduit (Gaurgaud 1991; Koyaguchi 1991).

The most striking field characteristics of the basaltic trachyandesitic ring dykes, ranging in thickness from 20 to 50 m, is that they are mainly exposed within the trachyandesite, and rarely within the rhyolite (Figures 2 & 4e). The basaltic trachyandesitic dykes typically shows an uncommon texture characterized by the existence of globular occurrences of dark greenish-grey pyroxenes set in a light yellowish-cream coloured plagioclase-rich groundmass. The size of these pyroxene clots ranges from 0.5 to 3 cm in diameter (Figure 4f).

The rhyolite and rhyolitic dykes have two separate and orthogonal joint systems oriented N60°E/60ºSE and N30ºW/75ºSW. The dips of these joint systems are almost vertical. In the mapped area the only possible fault has normal motion and cuts the Middle Eocene flyschoidal unit (Figure 2).

Analytical Techniques

Whole-rock geochemical analysis of 20 representative fresh samples, selected from a total of 85 rock specimens collected from the Orduzu volcanics, was performed at the ACME Analytical Laboratories Ltd. in Canada using Inductively Coupled Plasma-Atomic Emission Spectrometry (ICP-AES) for major elements and Inductively Coupled Plasma-Mass Spectrometry (ICP-MS) for trace and rare earth elements, respectively. 0.2 g rock powder sample was fused using lithium metaborate flux, and then major and trace-rare earth elements were analysed by ICP-AES, and ICP-MS, respectively; the standard sample SO-17 being used for quality assurance. For Mo, Cu, Pb, Zn, Ni, As, Cd, Sb, Bi, Ag, Au, Hg and Tl

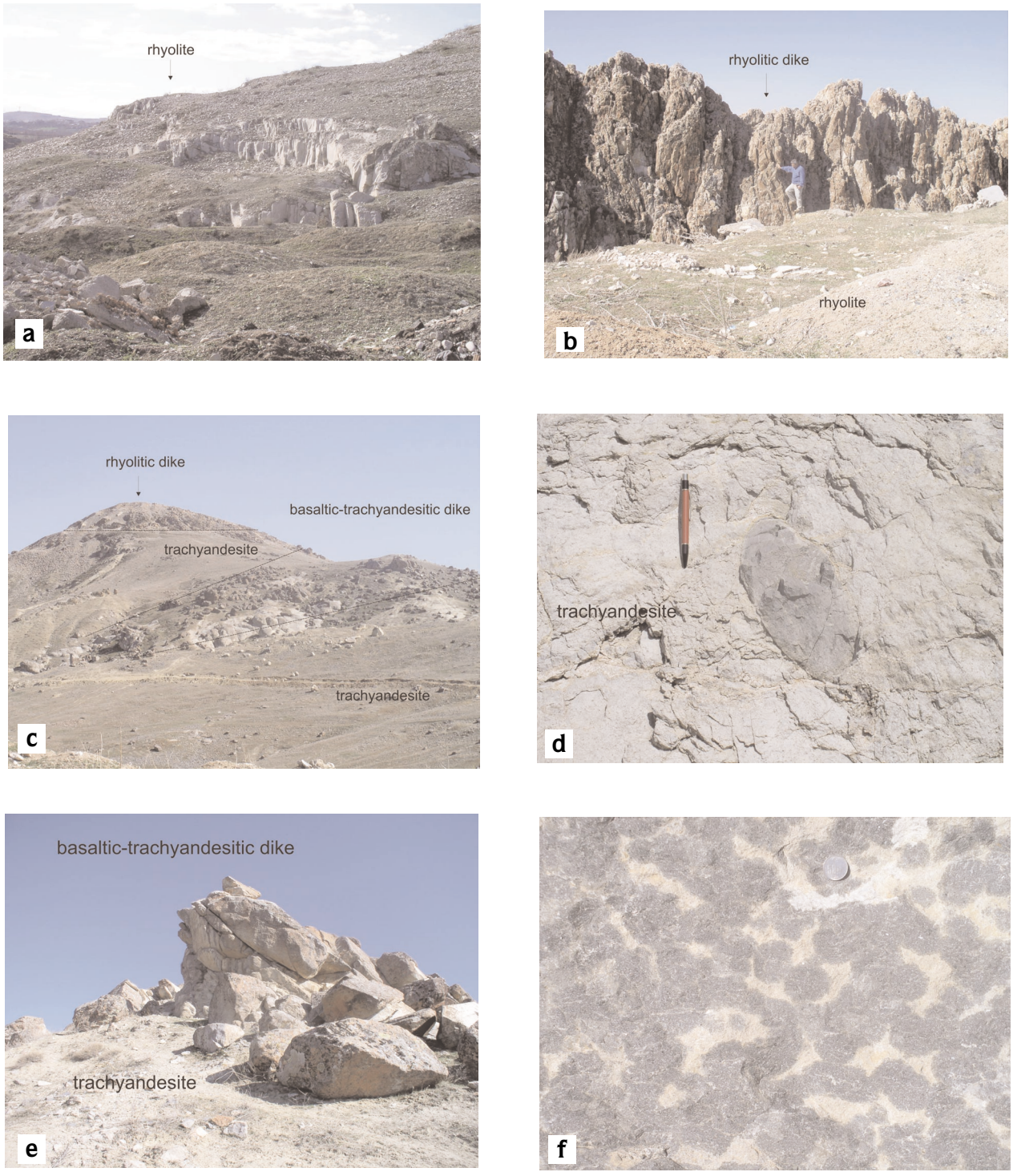

Figure 4. Field views of (a) rhyolite; (b) rhyolitic dyke; (c) rhyolitic dike, trachyandesite and basaltic trachyandesite dyke; (d) basaltic trachyandesite enclave in the trachyandesite; (e) basaltic trachyandesite dyke and (f) dark coloured globular pyroxene and biotite occurrences set in a light coloured groundmass in the basaltic trachyandesite dyke (diameter of coin is 17 mm).

analyses, 0.50 g of powdered sample was leached with 3 ml 2-2-2 HCl-HNO_3-H_2O at 95 °C for one hour, and then diluted to 10 ml, and analysed by ICP-MS; with the standard sample DS-4 used for quality assurance. Detection limits of the geochemical analyses are given in Table 1.

Table 1. Detection levels of elements during the geochemical analyses of rock samples.

Element	Detection Level	Element	Detection Level
SiO_2	0.02%	TiO_2	0.01%
Al_2O_3	0.03%	Fe_2O_3	0.04%
MnO	0.01%	MgO	0.01%
CaO	0.01%	Na_2O	0.01%
K_2O	0.04%	P_2O_5	0.01%
Cr_2O_3	0.001%	LOI	0.1%
Ba	5 ppm	Lu	0.01 ppm
Y	10 ppm	Zr	10 ppm
Ag	0.1 ppm	As	1 ppm
Bi	0.1 ppm	Cd	0.1 ppm
Co	0.5 ppm	Cs	0.1 ppm
Cu	0.1 ppm	Ga	0.5 ppm
Hf	0.5 ppm	Hg	0.1 ppm
Mo	0.1 ppm	Nb	0.5 ppm
Ni	0.1 ppm	Pb	0.1 ppm
Rb	0.5 ppm	Sb	0.1 ppm
Sn	1 ppm	Sr	0.5 ppm
Ta	0.1 ppm	Th	0.1 ppm
Tl	0.1 ppm	U	0.1 ppm
V	5 ppm	W	0.1 ppm
Y	0.1 ppm	Zn	1 ppm
Zr	0.5 ppm	La	0.5 ppm
Ce	0.5 ppm	Pr	0.02 ppm
Nd	0.4 ppm	Sm	0.1 ppm
Eu	0.05 ppm	Gd	0.05 ppm
Tb	0.01 ppm	Dy	0.05 ppm
Ho	0.05 ppm	Er	0.05 ppm
Tm	0.05 ppm	Yb	0.05 ppm

Five representative rock samples from the Orduzu volcanics have been selected for Electron Probe Microanalysis (EPMA). Polished thin sections were carbon coated and mineral chemical analyses were conducted using the electron probe facilities at the Earth and Atmospheric Sciences Department, University of Alberta, Canada. Mineral analyses were carried out using a JEOL JXA-8900 superprobe with five wavelength dispersive spectrometers, an energy dispersive spectrometer and cathode luminescence detector. The EPMA studies were performed under the conditions of 15 kV accelerating voltage, 15 nA current, 20 and 10 seconds counting times on peak and on each background, respectively, and PRZ correction (Armstrong 1995). Standards were natural minerals from the Smithsonian Institution collection of microbeam standards (Jarosewich 2002). Analytical errors are better than 1 % relative for major elements. F was calibrated using F-apatite (3.53 wt% F) as a standard, Cl was calibrated using tugtupite (7.58 wt% Cl) standard. Standard errors during standardization for F and Cl were 0.87% rel. and 0.55% rel., respectively.

Plagioclase separates from six rock samples analysed by the ^{40}Ar-^{39}Ar incremental heating method at the Nevada Isotope Geochronology Laboratory (NIGL) of the University of Nevada, Las Vegas, USA. Irradiations were performed in a dry tube device, shielded against thermal neutrons by a 5 mm thick jacket of B4C powder. J factors were determined by fusion of 3–5 individual crystals of neutron fluence monitors (Fish Canyon Tuff sanidine) that gave reproducibility's of 0.04% to 0.50% at each standard position. An uncertainty in J (flux parameter) of 0.5% was used in age determinations. Samples analysed by the furnace step heating method utilized a double vacuum resistance furnace similar to the Staudacher *et al.* (1978) design. Reactive gases were removed by a single MAP and two GP-50 SAES getters prior to being admitted to a MAP 215–50 mass spectrometer by expansion. Measured $^{40}Ar/^{36}Ar$ ratios were 289.97 ± 0.05% during this work, thus a discrimination correction of 1.01908 (4 AMU) was applied to measured isotope ratios. An age of 27.9 Ma (Steven *et al.* 1967; Cebula *et al.* 1986) was used for the Fish Canyon Tuff sanidine fluence monitor in calculating ages for samples. All analytical data are reported at a confidence level of 1s (standard deviation).

Petrography and Mineral Composition

The nomenclature of the Orduzu volcanics samples was established by means of geochemistry using the total alkalis versus silica (TAS) diagram of Le Bas *et al.* (1986). The textural and mineralogical characteristics of the studied volcanic rock samples are summarized in Table 2.

Rhyolite contains phenocrysts of plagioclase (Ø ~1.8 mm), sanidine (Ø ~0.07 to 0.25 mm), quartz (Ø ~0.5 mm), biotite and opaque minerals set in a groundmass of

Table 2. Textural and mineralogical features of the volcanic rocks from Orduzu, Malatya.

Rock type	Texture	Groundmass	Mineral composition and estimated modes
rhyolite	porphyritic (intergrowth of quartz and feldspar)	fine grained to cryptocrystalline	Pl: 40–50 %, An_{15-24} mainly oligoclase Sa: 20–30 % Qtz: 10–15 % Bt: ~5% Op: 1–2%
rhyolitic dyke	micrographic porphyritic	mainly medium to fine grained; rarely cryptocrystalline and even partly glassy	Pl: 30–35%, An_{20-34} mainly oligoclase Qtz: 15–20% Sa : 2–5% Bt: 1–3% Amp: 1–3% (only ghost amphiboles) Op: 2–5%
trachyandesite	hyalomicrolitic, microlitic porphyritic, fluidal	medium to fine grained; and partly glassy	Pl: 20–30%, An_{32-48} mainly andesine and labradorite Cpx: 5–20% Opx: 2–15% Hbl: 1–23% Bt: 2–25% Op: 3–5%
basaltic trachyandesite enclave	microlitic porphyritic, subophitic and fluidal	fine grained and partly glassy	Pl: 30–35%, An_{31-51} Cpx: 5–15% Opx : 3–5% Bt: 1–2% Op: 2–5%
basaltic trachyandesitic dyke	globular, microlitic, poikilitic, subophitic, porphyritic, clear core and sieved, trachytic and fluidal	medium to fine grained; and partly glassy, scarcely cryptocrystalline	Pl: 30–40%, An_{41-56} mainly andesine and labradorite Cpx: 5–20% Ne : 5–15% Bt: 1–10% Op: 2–5%

Explanation: Pl– plagioclase, Sa– sanidine, Qtz– quartz, Bt– biotite, Op– opaque, Cpx– clinopyroxene, Opx– orthopyroxene, Amp– amphibole, Ne– nepheline.

plagioclase, sanidine, quartz, biotite and opaque minerals. Some biotite flakes are prismatic in habit (Ø ~1.6 mm in length), whereas some others are stumpy (Ø ~2.2 mm). Some biotite phenocrysts are corroded phases in the rhyolite (Figure 5a). The groundmass locally displays spherulites formed from the intergrowth of K-feldspar and quartz.

Rhyolitic dykes have micrographic texture, and also contain some ghost amphibole and zoned plagioclase phenocrysts in contrast to the rhyolite flows. Some samples (OV-4, OV-22) include quartz phenocrysts, visible in hand specimen, which have been corroded and well rounded by resorption (Figure 5b). Sample OV-27 from these dykes includes plagioclase melting/dissolution, complex zoning and poikilitic textures (Figure 5c). These textural features may indicate magma mixing (e.g., Tsuchiyama 1985; Hibbard 1991; Feeley & Dungan 1996) or magma-early crystal interaction.

EPMA studies of the rhyolite (OV1) and rhyolitic dyke (OV4) show that the composition of plagioclase phenocrysts ranges from oligoclase (An_{15}) to andesine (An_{34}) in rhyolite and rhyolitic dykes (Table 3). However, the microlites in the rhyolite are mainly sanidine (Or_{77}). Biotites from the rhyolite and rhyolitic dykes have compositions of 60% and 57–70% phlogopite, respectively (Table 4). In the biotite mineral formula calculations (Table 4), the Si+Al (IV) sum is insufficient to fill the tetrahedral sites in microlites and microphenocrysts of biotite. This type of deficiency may be explained by the entry of high-charge cations (i.e. Ti^{4+} and Fe^{3+}) into the tetrahedral sites along with Si and Al(IV) (Farmer & Boettcher 1981; Brigatti *et al.* 1996).

Trachyandesites are microlitic, hyalo-microlitic and porphyritic (Table 2). The dominant phenocrysts are plagioclase (Ø ~3.2 mm) with zoning and spongy-cellular texture, biotite (Ø ~0.3 to 1.5 mm) with corroded margins and inclusions of opaque minerals, clinohypersthene (Ø ~0.9 mm), clinopyroxene (Ø ~0.45 to 1.2 mm) and amphibole (Ø ~0.1 to 2.3 mm). Amphibole is strongly corroded and surrounded by opaque minerals (Figure 5d). Some plagioclase phenocryts from the trachyandesites have mafic mineral inclusions (i.e. clinopyroxene) regularly arranged along the crystal margins (Figure 5e).

Basaltic trachyandesite enclaves are fine grained and comprise plagioclase, clinopyroxene, biotite and opaque minerals (Table 2).

Basaltic trachyandesitic dykes composed of plagioclase (Ø ~1.8 mm), clinopyroxene (Ø ~0.3 mm) and biotite (Ø ~0.35 to 0.9 mm) phenocrysts set in a plagioclase-rich groundmass with minor sanidine (Figure 5f). The clinopyroxenes and biotites also display subophitic textures with plagioclase within these mafic globular occurrences. The biggest phenocrysts are all plagioclase, typically exhibiting poikilitic textures with small inclusions of mafic minerals, mainly clinopyroxene. These mafic mineral inclusions exhibit systematic alignment along the margins of the embayed plagioclase phenocrysts (Figure 5g), with some randomly scattered (Figure 5h). The basaltic trachyandesitic dykes particularly differ from the trachyandesite as having some silica undersaturated minerals such as nepheline. Nepheline is generally found around the lath-shaped plagioclases, with an amount of up to 5% in volume, similar to monzonitic texture in plutonic and subvolcanic rocks.

EPMA results of plagioclases from the trachyandesite and basaltic trachyandesitic dykes yield the compositions of andesine (An_{31}) to labradorite (An_{56}) (Table 3). The plagioclase phenocrysts from the trachyandesite and basaltic trachyandesitic dykes are Ab rich at the rim (An_{38}), whereas some others are reversely zoned and are An rich at the rim (An_{51}) (Table 3). This may be interpreted as resulting from either partial dissolution during the magma mixing process (Feeley & Dungan 1996) (Table 3, sample OV-8) or a decompression effect.

The analysed biotite phenocrysts from the basaltic trachyandesitic dykes (OV-8) have a composition of 56% phlogopite with an enrichment in F content (Table 4). Pyroxene phenocrysts from the trachyandesite are represented by clinohypersthene (core En_{73}; rim En_{64}) (Table 4). In the basaltic trachyandesitic dykes, the pyroxenes in the groundmass and pyroxene inclusions within the biotites are composed of clinohypersthene ($Wo_{03}En_{58}Fs_{39}$) according to Morimoto (1988) classification, whereas the pyroxene inclusions within plagioclase phenocrysts are augite ($Wo_{40}En_{39}Fs_{21}$) and clinohypersthene ($Wo_{5-3}En_{53-58}Fs_{42-39}$) in composition (Table 4).

^{40}Ar-^{39}Ar Geochronology

In order to determine the timing of volcanism, five incremental $^{40}Ar/^{39}Ar$ dating was performed on the plagioclase separates from the different lithological units

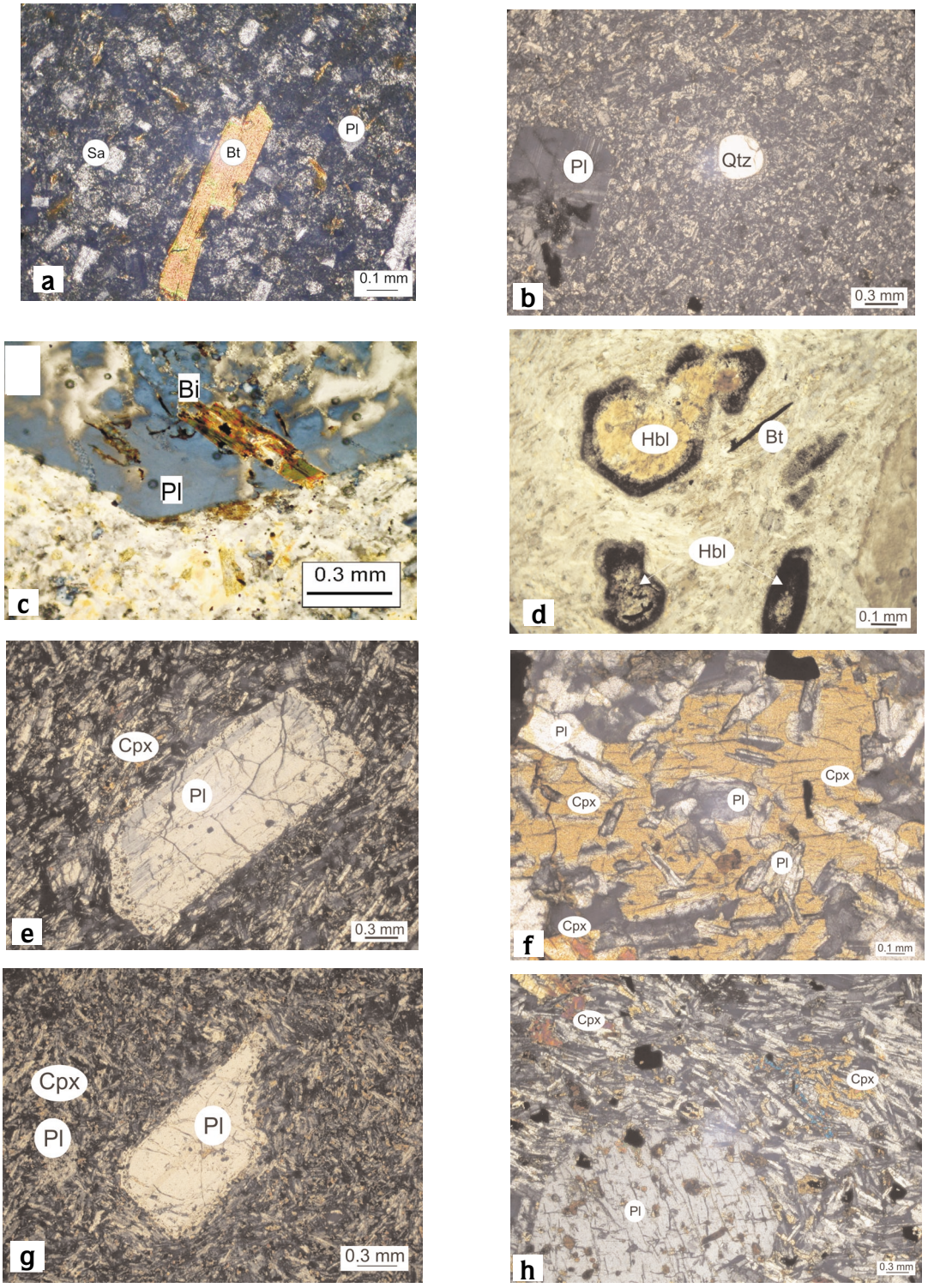

Figure 5. Photomicrographs showing **(a)** corroded biotite phenocrysts; **(b)** the corroded quartz phenocrysts; **(c)** dissolution/melting texture in the plagioclase phenocrysts; **(d)** corroded hornblendes; **(e)** mafic mineral inclusions in the plagioclase phenocrysts; **(f)** unusual poikilitic augite forming globular texture; **(g)** arrangement of mafic mineral inclusions within the corroded plagioclase phenocrysts; and **(h)** randomly scattered mafic mineral inclusions within the plagioclase phenocrysts. (Sa– sanidine; Bt– biotite; Pl– plagio clase; atz– quartz; Hbl– horn blende; Cpx– clinopyroxene).

Table 3. Representative electron micropobe analyses of plagioclases from the Orduzu volcanics. Atomic proportions on the basis of 32 oxygens.

Sample	OV1 Rhyolite				OV4 Rhyolitic dyke					OV16 Andesite				OV8 Basaltic trachyandesitic dyke						
Mineral	phenocryst			sa	mpc		phenocryst			phenocryst				megacryst (oscillatory – from core to rim						
Setting	c	m	r	mc	c	r	c	m	r	c	m	r	r	1	2	3	4	5	6	7
SiO_2	65.07	61.84	63.05	65.37	59.66	58.59	58.97	59.56	59.08	60.32	57.59	55.11	58.85	56.99	54.82	55.87	54.94	56.01	54.2	51.96
Al_2O_3	22.21	23.2	22.94	18.68	24.54	24.51	24.69	24.33	24.39	24.38	26.54	27.85	25.37	26.92	28.33	27.48	28.45	27.58	28.68	30.36
FeO	0.05	0.07	0.1	0.08	0.19	0.17	0.13	0.17	0.16	0.51	0.43	0.45	0.56	0.22	0.29	0.34	0.32	0.36	0.36	0.39
CaO	3.13	4.72	4.4	0.13	6.86	7.22	7.13	7	7.02	6.44	8.57	10.28	7.75	8.8	11.06	9.86	10.88	9.99	11.24	13.28
Na_2O	8.87	8.06	8.36	2.44	7.15	7.43	7.07	7.04	6.99	7.25	6.19	5.22	6.46	6.47	5.18	5.9	5.16	5.78	5.15	3.95
K_2O	1.04	0.89	0.88	12.64	0.91	0.76	0.92	0.92	0.9	0.79	0.51	0.36	0.59	0.69	0.47	0.58	0.5	0.57	0.41	0.26
BaO	0.04	0.03	0.16	0.36	n.a.	0.07	n.a.	n.a.	0.05	0.16	0.06	n.a.	0.07	0.01	n.a.	0.05	n.a.	0.03	0.03	n.a.
Total	100.4	99.46	99.89	99.7	99.31	98.75	98.91	99.02	98.59	99.85	99.89	99.27	99.65	100.1	100.15	100.08	100.25	100.32	100.07	100.2
Si	11.436	11.105	11.198	11.985	10.742	10.647	10.675	10.757	10.724	10.804	10.354	10.013	10.581	10.251	9.9	10.085	9.909	10.083	9.815	9.44
Al	4.6	4.91	4.801	4.036	5.207	5.249	5.267	5.178	5.217	5.146	5.623	5.963	5.375	5.707	6.03	5.846	6.047	5.851	6.121	6.5
Fe^{2+}	0.007	0.011	0.015	0.012	0.029	0.026	0.02	0.026	0.024	0.076	0.065	0.068	0.084	0.033	0.04	0.051	0.048	0.054	0.055	0.059
Ca	0.589	0.908	0.837	0.026	1.323	1.406	1.383	1.354	1.365	1.236	1.651	2.001	1.493	1.696	2.14	1.907	2.102	1.927	2.181	2.585
Na	3.022	2.806	2.878	0.867	2.496	2.618	2.481	2.465	2.46	2.518	2.158	1.839	2.252	2.256	1.81	2.065	1.804	2.017	1.808	1.391
K	0.233	0.204	0.199	2.956	0.209	0.176	0.212	0.212	0.208	0.18	0.117	0.083	0.135	0.158	0.11	0.134	0.115	0.131	0.095	0.06
Ba	0.003	0.002	0.011	0.026	0	0.005	0	0	0.004	0.011	0.004	0	0.005	0.001	-	0.004	0	0.002	0.002	0
Total	19.891	19.945	19.94	19.908	20.006	20.126	20.038	19.992	20.002	19.972	19.972	19.967	19.925	20.102	20.04	20.091	20.027	20.065	20.076	20.036
X_{An}	0.153	0.232	0.214	0.007	0.329	0.335	0.339	0.336	0.338	0.314	0.421	0.51	0.385	0.549	0.863	0.464	0.523	0.473	0.534	0.64
X_{Ab}	0.786	0.716	0.735	0.225	0.62	0.623	0.609	0.611	0.61	0.64	0.55	0.469	0.58	0.412	0.085	0.503	0.449	0.495	0.443	0.345
X_{Kfs}	0.061	0.052	0.051	0.768	0.052	0.042	0.052	0.053	0.052	0.046	0.03	0.021	0.035	0.039	0.052	0.033	0.029	0.032	0.023	0.015

Sa– sanidine, mpc– microphenocryst, c– core, m– middle; r– rim, mc– microlite, 1–7– from core to rim; n.a., not analysed.
Plagioclase, X_{An}: Ca/ (K+Na+Ca), X_{Ab}: Na/(K+Na+Ca), Sanidine, X_{Kfs}: K/(K+Na+Ca)

Table 4. Representative electron micropobe analyses of pyroxene and biotite. Atomic proportions on the basis of 6 oxygens and 11 oxygens for pyroxene and biotite, respectively.

Sample	OV16 Andesite				OV8 Basaltic trachyandesitic dyke				Sample	OV21 Rhyolite				OV4 Rhyolitic dyke			OV8 Bas. trachyandesitic dyke		
Mineral	chyp – (core to rim)				chyp	chyp	cpx	chyp	Mineral	biotite		botite		biotite			biotite		
Setting	1	2	3	4	gm	ip	ip	ib	Setting	c	r	c	r	mpc	mpc	mc	mc	mc	mc
SiO_2	53.94	52.85	52.65	52.39	52.71	52.68	51.86	52.37	SiO_2	36.11	36.20	36.16	35.98	34.09	34.33	37.10	37.35	37.49	37.68
TiO_2	0.15	0.15	0.08	0.13	0.35	0.06	0.44	0.29	TiO_2	3.27	3.54	3.08	3.21	4.37	4.22	2.57	6.24	5.97	6.06
Al_2O_3	2.45	2.60	1.46	1.51	0.50	0.23	0.99	0.45	Al_2O_3	14.84	14.88	14.76	14.61	14.49	14.62	12.61	11.85	12.00	12.07
Cr_2O_3	0.27	0.18	0.05	0.06	0	0	0	0	FeO	13.17	13.48	13.08	13.09	14.08	14.16	11.06	13.94	14.17	14.30
FeO	13.05	16.17	20.40	21.50	24.41	25.84	12.44	24.94	MnO	0.25	0.20	0.22	0.24	0.24	0.25	0.16	0.05	0.05	0.05
MnO	0.26	0.28	0.34	0.41	0.52	0.7	0.36	0.53	MgO	16.08	15.89	16.23	16.18	14.89	15.14	18.62	14.93	14.96	15.06
MgO	28.75	26.71	24.12	23.26	20.56	18.96	13.89	21.20	Na_2O	0.58	0.64	0.63	0.56	0.58	0.60	0.49	0.51	0.42	0.41
CaO	1.14	1.01	1.03	1.20	1.52	2.39	19.79	1.52	K_2O	9.06	9.14	8.85	9.19	9.28	9.27	9.63	8.78	9.17	8.91
Na_2O	0.04	0.03	0	0.02	0	0.02	0.29	0.02	F	4.80	4.72	4.88	4.76	5.24	5.23	6.50	1.32	1.28	1.24
K_2O	0	0.02	0	0	0	0.05	0.06	0.02	Cl	0.15	0.16	0.15	0.10	0	0.02	0.02	0.31	0.26	0.25
Total	100.05	100.00	100.13	100.48	100.57	100.93	100.12	101.34	Total	98.31	98.85	98.04	97.92	97.26	97.84	98.76	95.28	95.77	96.03
Si	1.927	1.917	1.945	1.940	1.978	1.989	1.956	1.957	Si	2.730	2.723	2.739	2.733	2.648	2.649	2.822	2.822	2.824	2.824
Ti	0.004	0.004	0.002	0.004	0.010	0.002	0.012	0.008	Al [IV]	1.270	1.277	1.261	1.267	1.327	1.330	1.131	1.055	1.065	1.066
Al	0.103	0.111	0.064	0.066	0.022	0.010	0.044	0.020	Cation deffiency at tetrahedral site	0.000	0.000	0.000	0.000	0.025	0.021	0.047	0.123	0.111	0.109
Cr	0.008	0.005	0.001	0.002	0.000	0.000	0.000	0.000	Al [VI]	0.053	0.042	0.056	0.040	0.000	0.000	0.000	0.000	0.000	0.000
Fe^{2+}	0.390	0.490	0.630	0.666	0.766	0.816	0.392	0.779	Ti	0.186	0.200	0.175	0.183	0.255	0.245	0.147	0.355	0.338	0.342
Mn	0.008	0.009	0.011	0.013	0.017	0.022	0.011	0.017	Fe^{2+}	0.833	0.848	0.828	0.831	0.915	0.914	0.704	0.881	0.893	0.896
Mg	1.531	1.444	1.328	1.284	1.150	1.067	0.781	1.181	Mg	1.813	1.782	1.833	1.832	1.725	1.742	2.112	1.682	1.680	1.683
Ca	0.044	0.039	0.041	0.048	0.061	0.097	0.800	0.061	Mn	0.016	0.013	0.014	0.015	0.016	0.016	0.010	0.003	0.003	0.003
Na	0.003	0.002	0.000	0.001	0.000	0.001	0.021	0.001	K	0.874	0.877	0.855	0.890	0.920	0.913	0.935	0.846	0.881	0.852
K	0.000	0.001	0.000	0.000	0.000	0.002	0.003	0.001	Na	0.170	0.187	0.185	0.165	0.175	0.180	0.145	0.149	0.123	0.119
Total	4.016	4.023	4.021	4.023	4.003	4.006	4.021	4.025	Total	7.944	7.949	7.947	7.958	7.980	7.987	8.005	7.794	7.807	7.786
X_{Wo}	0.022	0.020	0.020	0.024	0.031	0.049	0.405	0.030	X_{Ann}	0.287	0.294	0.285	0.286	0.314	0.313	0.237	0.302	0.306	0.307
X_{En}	0.779	0.732	0.664	0.643	0.582	0.539	0.396	0.584	X_{Phl}	0.625	0.618	0.930	0.631	0.593	0.597	0.710	0.576	0.576	0.576
X_{Fs}	0.199	0.248	0.315	0.333	0.387	0.412	0.199	0.386	Mg #	0.685	0.678	0.689	0.688	0.653	0.656	0.750	0.656	0.653	0.652
Mg #	0.797	0.747	0.678	0.659	0.600	0.567	0.666	0.602											

chyp– clinohyperstene, gm– groundmass, ip– inclusion in plagioclase, ib– inclusion in biotite, c– core, r– rim, mc– microlite, mpc– microphenocryst, 1–4– from core to rim. X_{Wo}: Ca/(Fe+Mg+Ca); X_{En}: Mg/(Fe+Mg+Ca); X_{Fs}: Fe/(Fe+Mg+Ca); X_{Phl}: $Mg/(Al^{VI}+Fe^{2+}+Mg)$; X_{Ann}: $Fe^{2+}/(Al^{VI}+Fe^{2+}+Mg)$; Mg # = Mg / $(Mg^{2+}+Fe^{2+})$.

(Table 5; Figure 6). The plagioclase separate of sample OV-13 collected from trachyandesite yielded a meaningless older age due to excess radiogenic Ar, so that the initial $^{40}Ar/^{36}Ar$ in the sample is ~340, and it has been excluded from the dataset.

The OV-21 plagioclase separate from the rhyolite gave plateau and total gas ages of 15.88 ± 0.07 and 16.12 ± 0.08 Ma, respectively (Table 5). The OV-38 plagioclase separate from the rhyolite yielded a good plateau age of 16.08 ± 0.08 Ma, which is indistinguishable from the 16.10 ± 0.08 Ma total gas age (Table 5; Figure 6). The age spectrum is almost ideally flat (concordant ages). The OV-17 plagioclase separate from the rhyolitic dykes gave both an isochron and a plateau age (Table 5; Figure 6). The isochron age of 15.82 ± 0.04 Ma is slightly younger than the plateau age (16.00 ± 0.10 Ma) and the total gas age (16.15 ± 0.10 Ma), and shows that the sample contains some excess argon ($^{40}Ar/^{36}Ar$ = 318). The isochron age of 15.82 ± 0.04 Ma is considered to be the most accurate age for this sample (Figure 6). The OV-20 plagioclase separate from the rhyolitic dykes gave a plateau age of 16.19 ± 0.01 Ma (Table 5; Figure 6). The age spectrum is slightly U-shaped, suggesting some excess argon may be present. Thus, the total gas age of 16.55 ± 0.08 Ma may overestimate the true age (Figure 6). The OV-8 plagioclase separate from the basaltic trachyandesitic dykes gave a plateau age (steps from 3 to 9) of 15.97 ± 0.09 Ma (Table 5; Figure 6). The age spectrum exhibits high initial ages (to 149 Ma) falling to a minimum of 15.8 Ma with the 6th step, and rising slightly to final step ages just over 16 Ma (Table 5). Again, the shape of the age spectrum is U-shaped, suggesting excess argon may be present (Figure 6). The most conservative interpretation is that the sample is younger than the minimum age on the age spectrum, so is <15.8 Ma (Figure 6).

All the age values indicate that the volcanism in the Orduzu area occurred during the Middle Miocene, and is similar in age to volcanism described from different parts of the Yamadağ area (i.e. Leo *et al*. 1974; Arger *et al*. 2000; Kürüm *et al*. 2004; see Figure 1b).

Whole-rock Geochemistry

Whole-rock major, trace and REE geochemical compositions of the representative rock samples from the Orduzu volcanics are given in Table 6. Rhyolite, rhyolitic dykes and trachyandesite are characterized by subalkaline and calc-calkaline (Irvine & Baragar 1971) geochemical affinities. The exceptions, however, are the basaltic trachyandesitic dykes which plot in the alkaline sub-field close to the dividing line between the alkaline and subalkaline compositions (Figure 7a). All these samples plot in the high-K subfield in the K_2O-SiO_2 diagram of Le Maitre *et al*. (1989), except for one enclave sample which plots in the medium-K subfield (Figure 7b).

The rhyolites/rhyolitic dykes and trachyandesites/ basaltic trachyandesitic dykes constitute discrete associations in the major and trace element vs silica variation diagrams (Figure 8). However, trachyandesites differ from basaltic trachyandesitic dykes in having a wider compositional range. Thus, it is concluded that two discrete less-evolved magmas were involved in the genesis of the trachyandesites and basaltic trachyandesitic dykes of the Orduzu volcanics; one of which was calc-alkaline (trachyandesite), whereas the other was mildly alkaline in composition (the basaltic trachyandesitic dykes). Among the Large Ion Lithophile Elements (LILE), Rb and Ba contents of the trachyandesite and basaltic trachyandesitic dykes are apparently less than those of the rhyolite and rhyolitic dykes; but Sr content is higher (Figure 8). The Rb and Ba contents of the trachyandesite are nonetheless significantly enriched relative to those in the basaltic trachyandesitic dikes (Figure 8).

High Field Strength Elements (HFSE), such as Nb, Y, Hf and Zr, seem to be unexpectedly enriched in the trachyandesite and basaltic trachyandesitic dykes relative to the rhyolite and rhyolitic dykes, but their concentrations of Th and U are reversed (Figure 8, Table 6). This may reflect melt generation by variable partial melting of the same source (e.g., Pearce *et al*. 1990). However, the basaltic trachyandesitic dykes exhibit enrichment in Nb, Y and depletion in Hf, Zr relative to trachyandesite (Figure 8). The basaltic trachyandesite enclave always plots with the trachyandesite and basaltic trachyandesitic dykes in Figure 8. This may indicate mixing and mingling between the coeval magma sources of the trachyandesite and basaltic trachyandesitic dykes. A somewhat similar mechanism was proposed by Screiber *et al*. (1999) for the Tertiary Westerwald subvolcanic complex in Germany, where magma mixing between trachytic and latitic magmas has yielded centimetre-sized dark coloured globular aggregates similar to those in the Orduzu volcanic system.

Table 5. Ar-Ar data for plagioclase seperates from the volcanic rocks of Orduzu, Malatya.

T ºC	$^{40}Ar/^{39}Ar$	$^{37}Ar/^{39}Ar$	$^{36}Ar/^{39}Ar$	% ^{40}Ar*	Ca/K	% ^{39}Ar rlsd	Age (±σ) (Ma)
OV21 (rhyolite) 26.20 mg, J= 0.001572 ± 0.5%, total gas age 16.12 ± 0.08, plateau age (steps 3–7) 15.88 ± 0.07							
650	108.057	0.920	0.335	10.0	4.848	1.5	30.27±0.29
730	18.877	1.057	0.045	31.8	5.572	3.4	16.69±0.22
810	7.153	1.202	0.006	80.8	6.340	6.3	15.92±0.12
890	6.714	1.361	0.004	85.8	7.176	8.7	15.99±0.10
960	6.702	1.487	0.005	85.5	7.846	9.6	15.94±0.09
1030	6.364	1.552	0.004	89.5	8.186	10.9	15.88±0.12
1100	6.353	1.621	0.004	88.9	8.552	11.6	15.76±0.09
1180	6.280	1.702	0.004	90.3	8.980	12.8	15.73±0.09
1250	6.243	1.735	0.003	92.0	9.156	14.4	15.96±0.09
1340	6.653	1.736	0.004	87.2	9.162	12.4	16.10±0.11
1400	6.791	1.795	0.006	83.2	9.475	8.3	15.50±0.09
OV38 (rhyolite) 23.95 mg, J= 0.001575 ± 0.5%, total gas age 16.10±0.08, plateau age (steps 6–9) 16.08±0.08							
650	28.875	0.236	0.076	23.7	1.221	0.9	19.22±0.15
730	8.511	0.303	0.010	68.7	1.569	2.2	16.32±0.09
810	6.733	0.323	0.004	84.9	1.674	4.5	16.08±0.09
890	6.650	0.310	0.003	86.6	1.607	7.5	16.27±0.09
960	6.346	0.252	0.002	90.4	1.305	10.3	16.23±0.08
1030	5.885	0.186	0.001	96.4	0.963	14.5	16.05±0.08
1100	5.833	0.157	0.001	96.9	0.812	16.8	16.00±0.08
1180	5.997	0.174	0.001	94.2	0.904	17.9	16.00±0.08
1260	6.154	0.210	0.002	92.2	1.091	19.3	16.06±0.08
1340	6.530	0.430	0.003	87.2	2.232	4.7	15.92±0.08
1400	7.084	0.395	0.005	83.9	2.046	1.3	15.99±0.14
OV17 (rhyolitic dike) 23.96 mg, J= 0.001570 ± 0.5%, total gas age 16.15 ± 0.10, plateau age (steps 2–9) 16.00 ± 0.10, isochron age: 15.82 ± 0.04							
650	31.804	0.452	0.084	23.6	2.696	2.3	21.05±0.34
730	7.596	0.453	0.007	76.4	2.702	5.7	16.18±0.14
810	6.221	0.503	0.002	91.4	3.002	11.0	15.94±0.11
890	6.146	0.557	0.002	92.2	3.325	15.0	15.93±0.11
960	6.237	0.637	0.003	90.6	3.803	14.4	15.89±0.11
1030	6.276	0.723	0.003	90.5	4.315	12.3	15.95±0.11
1100	6.610	0.803	0.004	86.6	4.791	9.2	16.03±0.11
1170	7.034	0.739	0.005	82.0	4.411	8.5	16.13±0.12
1240	7.198	0.750	0.006	80.0	4.474	8.7	16.11±0.12
1320	6.954	0.911	0.005	84.9	5.438	7.9	16.44±0.12
1400	6.770	0.978	0.005	86.6	5.841	5.0	16.13±0.11
T ºC	$^{40}Ar/^{39}Ar$	$^{37}Ar/^{39}Ar$	$^{36}Ar/^{39}Ar$	% ^{40}Ar*	Ca/K	% ^{39}Ar rlsd	Age (±σ) (Ma)

Table 5. (Continued)

T ºC	$^{40}Ar/^{39}Ar$	$^{37}Ar/^{39}Ar$	$^{36}Ar/^{39}Ar$	% ^{40}Ar*	Ca/K	% ^{39}Ar rlsd	Age (±σ) (Ma)
OV20 (rhyolitic dike) 23.50 mg, J= 0.001565 ± 0.5%, total gas age 16.55 ± 0.08, plateau age (steps 3–8) 16.19 ± 0.01							
650	103.710	1.235	0.314	12.2	6.545	1.3	35.47±0.43
730	12.386	1.424	0.022	51.8	7.548	3.3	17.63±0.10
810	7.951	1.200	0.008	75.6	6.357	7.2	16.65±0.11
890	7.050	1.216	0.005	83.0	6.444	10.5	16.29±0.09
960	6.899	1.263	0.005	82.9	6.695	12.1	15.95±0.09
1030	6,853	1.290	0.005	83.7	6.835	13.1	16.02±0.09
1100	7.244	1.293	0.006	79.6	6.852	13.0	16.12±0.09
1170	7.917	1.264	0.008	74.2	6.700	12.3	16.34±0.09
1240	7.660	1.307	0.007	77.3	6.927	11.0	16.41±0.09
1320	7.735	1.367	0.007	76.9	7.243	9.7	16.44±0.09
1400	7.973	1.375	0.008	74.4	7.287	6.5	16.23±0.11
OV8 (basaltic-trachyandesitic dike), 10.77 mg, J= 0.001551 ± 0.5%, total gas age 18.97 ± 0.08, plateau age (steps 3–9) 15.97 ± 0.09							
650	506.752	0.981	1.557	10.9	5.297	1.9	148.75±1.38
730	27.895	0.945	0.070	27.6	5.104	4.4	21.26±0.32
810	16.462	0.849	0.035	39.1	4.581	8.8	17.84±0.15
890	12.459	0.783	0.023	47.6	4.227	13.3	16.47±0.09
960	9.395	0.775	0.013	61.9	4.182	13.9	16.10±0.09
1030	7.270	0.807	0.006	79.0	4.355	12.3	15.82±0.09
1100	6.992	0.838	0.005	82.8	4.526	10.2	15.87±0.08
1180	7.166	0.598	0.005	81.6	3.225	13.2	15.99±0.10
1250	7.568	0.733	0.007	77.9	3.956	10.3	16.04±0.09
1340	9.163	1.405	0.013	64.8	7.593	6.0	16.00±0.10
1400	9.439	1.615	0.014	63.0	8.729	5.7	16.03±0.16
OV13 (basaltic-trachyandesitic dike), 19.02 mg, J= 0.001552 ± 0.5%, total gas age 58.11 ± 0.13, no plateau and isochron age							
730	927.252	2.422	2.781	13.1	13.023	8.4	313.40±3.14
810	73.401	2.168	0.213	16.6	11.654	11.2	33.90±0.44
890	68.013	2.100	0.190	19.4	11.284	15.7	36.85±0.22
960	41.380	2.103	0.109	24.7	11.301	15.7	28.50±0.16
1030	133.509	2.134	0.374	19.1	11.468	12.7	70.45±0.47
1100	40.697	1.483	0.107	24.7	11.004	9.5	38.83±0.28
1170	14.567	1.822	0.029	45.8	9.787	8.0	18.34±0.12
1240	16.994	2.057	0.038	38.6	11.053	6.3	18.01±0.13
1400	17.429	2.532	0.039	38.9	13.620	12.4	18.82±0.11

Explanation: rlsd– released, isotope beams in mV– error in age includes 0.5% J error– all errors 1 sigma, not corrected for decay. 4 amu discrimination: 1.01908 ± 0.005%; $^{40/39}K$= 0.0002 ± 0.0003; $^{36/37}Ca$= 0.000278 ± 2.89%; $^{39/37}Ca$= 0.00067 ± 1.96%.

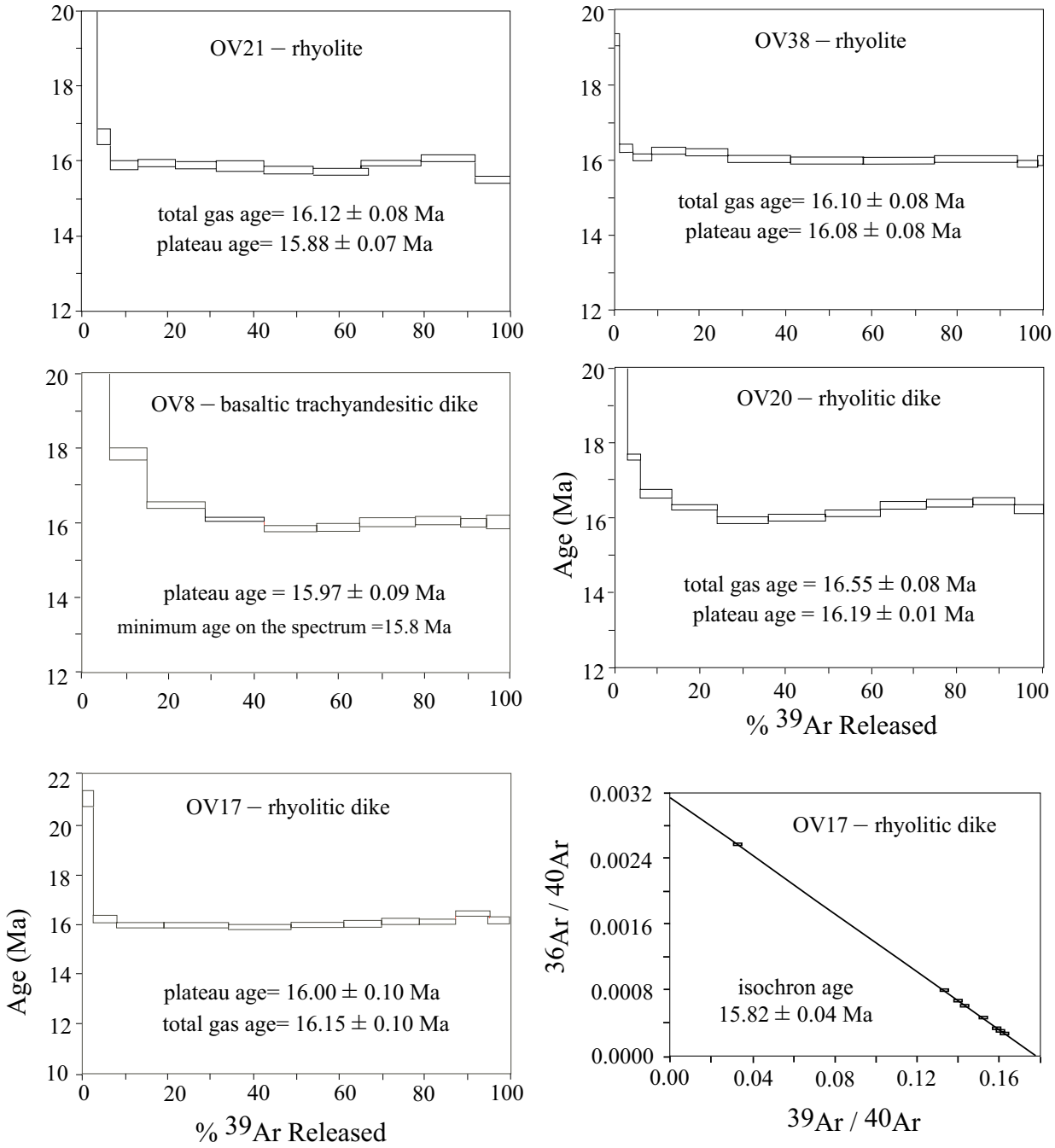

Figure 6. ^{40}Ar-^{39}Ar age spectrum of the rhyolite, rhyolitic dyke, basaltic trachyandesitic dyke and isochron age of the rhyolitic dyke.

Primordial mantle normalized (Sun & McDonough 1989) spider diagrams show that rhyolite and rhyolitic dykes have similar patterns, with considerable Ba, Nb, P and Ti negative anomalies, but a positive anomaly in K content (Figure 9a). Rhyolitic rocks are enriched in LILE (Cs, Rb, Ba, K, Th, U) and slightly depleted in Hf, Zr (HFSE). In the trachyandesites and basaltic trachyandesitic dykes Ba and Nb show negative anomalies, although they are less pronounced than those in the rhyolites and rhyolitic dykes (Figure 9b).

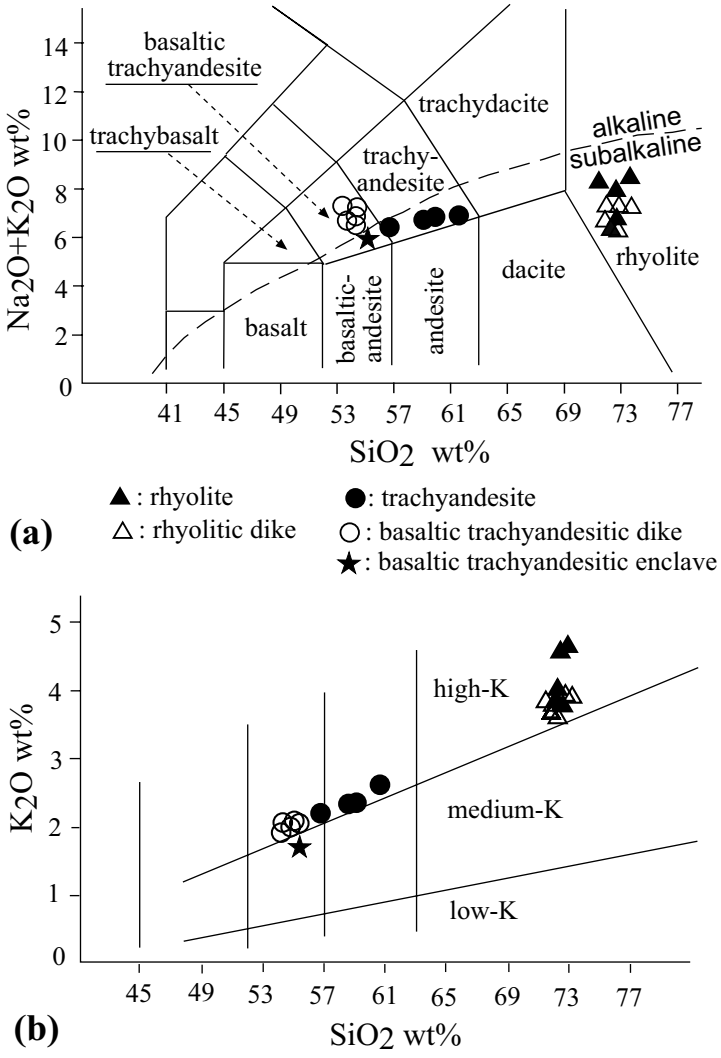

Figure 7. Chemical classification of the rock samples from the Orduzu volcanics **(a)** in the TAS diagram of Le Bas *et al.* (1986) and **(b)** in SiO_2 vs K_2O diagram.

Trachyandesites and basaltic trachyandesitic dykes differ from the rhyolitic rocks in having positive Pb and Sr anomalies. In particular, the basaltic trachyandesitic dike samples OV8 and OV13 contain high Pb and Sr compared to the andesitic samples (Figure 9b). Furthermore, OV8 also has the highest Cs content of all the samples (Figure 9b).

Chondrite-normalized (Sun & McDonough 1989) REE plots indicate that rhyolitic rocks are enriched in Light Rare Earth Elements (LREE), especially La and Ce; but may be slightly depleted in Nd, Sm, Eu (Middle Rare Earth Element; MREE), and all Heavy Rare Earth Element (HREE) from Gd to Lu, compared to trachyandesites and basaltic trachyandesitic dykes (Table 6; Figure 9c, d). Rhyolite and rhyolitic dyke samples display an apparent fractionation from LREE to MREE with a negative Eu anomaly (Eu/Eu*= 0.57–0.81 in rhyolites; 0.71–0.92 in rhyolitic dykes), which may be interpreted as signifying the evolved magma compositions in the genesis of these felsic rock associations (Figure 9c). This is also shown by the higher LREE and MREE contents of the rhyolitic dykes compared to those in the rhyolites (Table 6; Figure 9c). Trachyandesites and basaltic trachyandesitic dykes show a fractionation from LREE to MREE without any Eu anomaly (Eu/Eu*= 0.86–1.02 in trachyandesites;

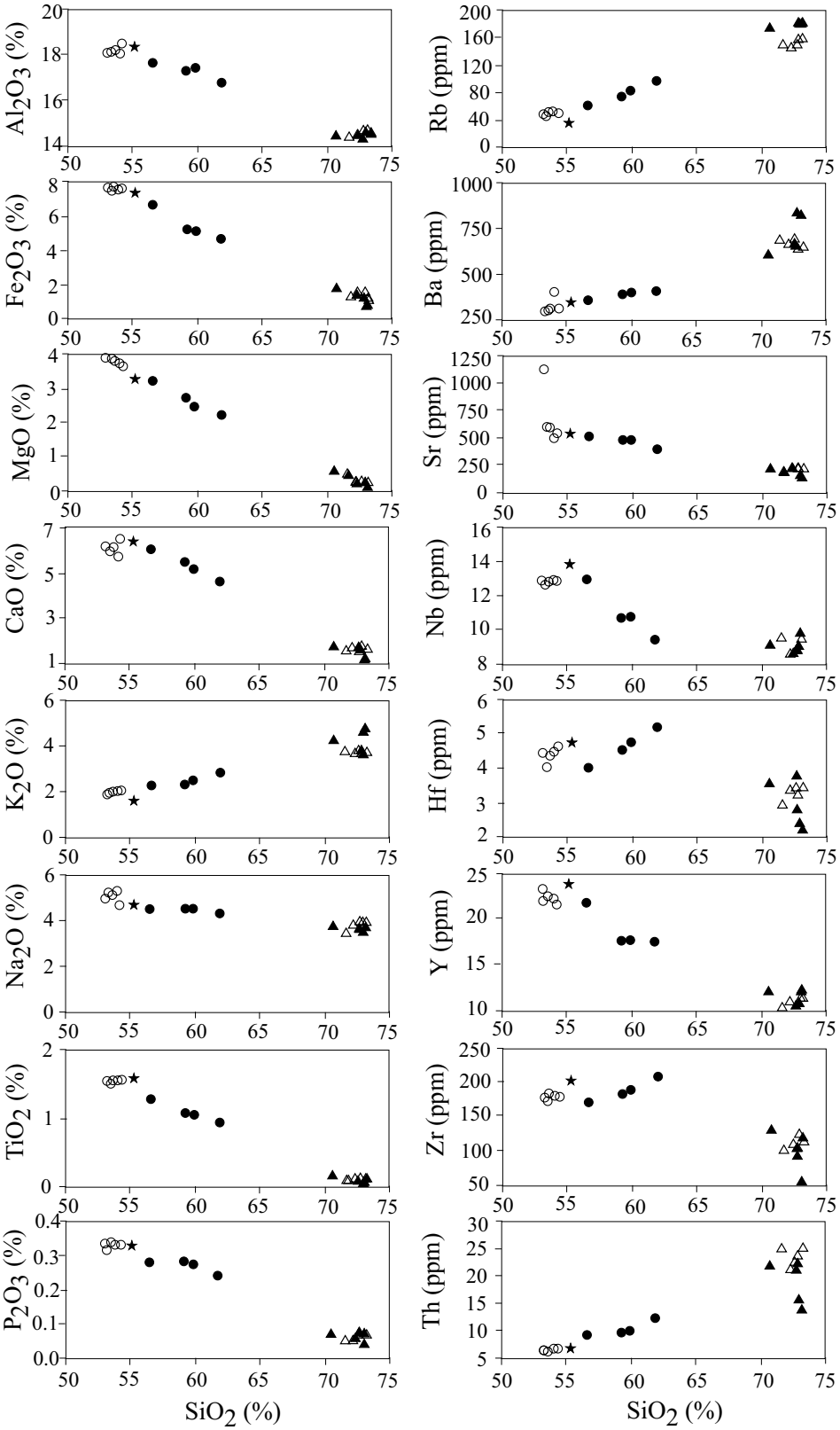

Figure 8. Major oxides and some trace elements vs SiO_2 variation diagrams. For legend see Figure 7.

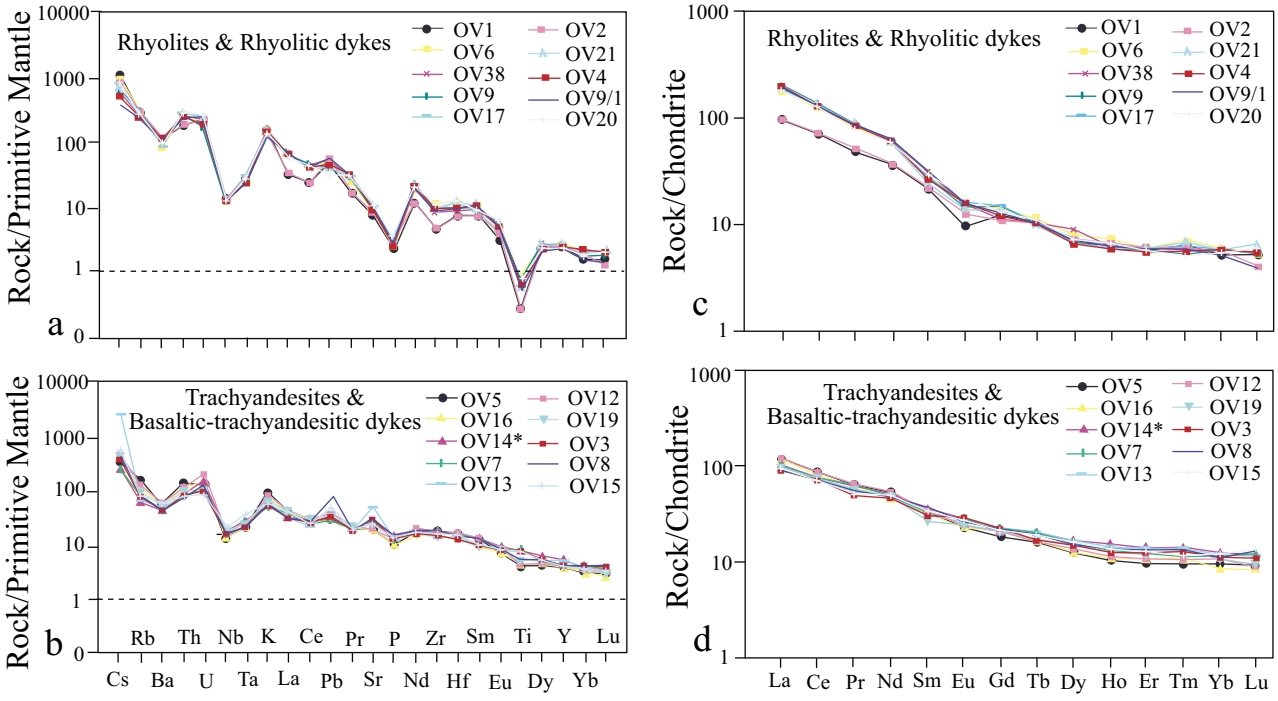

Figure 9. (**a**, **b**) Prim-normalized trace and (**c**, **d**) chondrite-normalized rare earth element spider diagrams. Normalizing values after Sun & McDonough (1989). See Table 6 for explanation of sample number.

0.96–1.05 in basaltic trachyandesitic dykes), and a slight fractionation from MREE to HREE (Figure 9d).

The REE, LILE and HFSE geochemical composition of OV-14 (the basaltic trachyandesite enclave found within the trachyandesite) is similar to that of the basaltic trachyandesitic dykes (Figure 9b, d).

Discussion

Field, mineralogical, petrographical and geochemical studies have concluded that the rhyolite and rhyolitic dykes were derived from a distinct felsic magma source. Trachyandesite and basaltic trachyandesitic dykes originated from a calc-alkaline mafic melt and a discrete mildly alkaline basaltic magma, respectively. The petrogenesis and solidification processes which may have modified the magma compositions will be briefly discussed below.

Rhyolitic Rocks

In the field, rhyolite and rhyolitic dikes were observed to be the earliest units of the Orduzu volcanic system, cut by trachyandesite and basaltic trachyandesitic dykes.

The enrichment in Rb, Ba, K, Th and LREE and the depletion in Nb, Y, Hf, Zr and Ti in the rhyolite and rhyolitic dykes can be interpreted to have been inherited either from an enriched mantle source metasomatized by earlier subduction-derived fluids, or from a crustal origin. For example, if the rhyolitic lavas were derived from low degree melts of the metasomatized mantle, in addition to LILE and LREE, they would have also been enriched in MgO content. But, their MgO content is very low, ranging from 0.14 to 0.60 wt% (Table 5). Moreover, as the rhyolitic rocks are the oldest units in the mapped area, they cannot have been derived by fractional crystallization from the mafic magma sources of the younger trachyandesite lava or basaltic trachyandesite dykes. Therefore, the rhyolites of the Orduzu volcanics must have been derived from a distinct magma source that was possibly generated by the partial melting of crustal rocks, probably caused by the heat associated with mafic melt injection into the crust. The enrichment in Rb, Ba, Th, K and depletion in Sr, Ti and a slight negative Eu anomaly in the Prim-normalized REE spider diagram may be considered as consistent with such a crustal derivation for the rhyolitic rocks of the Orduzu volcanics.

Table 6. Whole-rock major (wt %) and trace (ppm) element geochemical composition.

Sample	OV1	OV2	OV6	OV21	OV38	OV4	OV9	OV9/1	OV17	OV20	OV5	OV12	OV16	OV19	OV14*	OV3	OV7	OV8	OV13	OV15
	Rhyolite					Rhyolitic dyke					Trachyandesite					Basaltic trachyandesitic dike				
SiO_2	73.10	72.96	70.63	72.68	72.75	72.30	72.65	71.63	73.20	72.83	61.89	59.92	59.26	56.60	55.04	53.40	54.28	53.65	53.21	54.02
TiO_2	0.06	0.06	0.20	0.13	0.11	0.14	0.13	0.13	0.14	0.15	0.92	1.02	1.07	1.26	1.57	1.49	1.54	1.53	1.52	1.52
Al_2O_3	14.73	14.73	14.54	14.46	14.39	14.52	14.66	14.44	14.67	14.60	16.70	17.38	17.26	17.63	18.35	18.11	18.45	18.16	18.00	17.95
tFe_2O_3	0.96	0.89	1.93	1.47	1.35	1.53	1.44	1.37	1.18	1.53	4.60	5.06	5.24	6.60	7.41	7.59	7.53	7.70	7.62	7.47
MnO	0.03	0.03	0.05	0.03	0.03	0.02	0.02	0.02	0.01	0.02	0.05	0.05	0.05	0.09	0.09	0.10	0.09	0.10	0.10	0.10
MgO	0.14	0.20	0.60	0.29	0.28	0.26	0.22	0.47	0.21	0.25	2.14	2.40	2.67	3.19	3.25	3.83	3.59	3.75	3.92	3.70
CaO	1.11	1.10	1.82	1.72	1.54	1.67	1.59	1.59	1.63	1.76	4.56	5.17	5.42	6.03	6.43	5.90	6.49	6.11	6.12	5.68
Na_2O	3.75	3.53	3.72	3.77	3.64	3.86	3.90	3.43	3.92	3.91	4.24	4.40	4.38	4.37	4.62	5.10	4.58	4.94	4.85	5.16
K_2O	4.81	4.71	4.24	3.67	3.82	3.68	3.79	3.75	3.73	3.65	2.71	2.39	2.20	2.13	1.56	1.80	1.97	1.94	1.83	1.93
P_2O_5	0.05	0.07	0.08	0.07	0.07	0.06	0.08	0.06	0.07	0.08	0.24	0.27	0.28	0.28	0.33	0.31	0.33	0.34	0.33	0.33
Cr_2O_3	b. d.	b. d.	b. d.	b. d.	0.001	b. d.	b. d.	b. d.	0.002	b. d.	0.001	0.002	0.003	0.001	b. d	0.002	b. d	b. d	0.001	0.001
LOI	1.1	1.6	2.0	1.6	1.9	1.8	1.4	3.0	1.1	1.1	1.8	1.8	2.0	1.7	1.2	2.2	1.0	1.6	2.3	2.0
Total	99.94	99.98	99.88	99.97	99.96	99.92	99.95	99.96	99.93	99.95	99.89	99.91	99.88	99.93	99.90	99.87	99.89	99.85	99.83	99.90
Trace elements																				
Ni	1.1	0.7	3.5	0.3	2.1	0.8	0.9	1.3	0.6	1.3	10.7	11.7	11.1	8.0	5.7	8.1	5.5	8.0	7.6	5.6
Cr	b. d.	b. d.	b. d.	b. d.	6.84	b. d.	b. d.	b. d.	13.68	b. d.	6.84	13.68	20.53	6.84	b. d.	13.68	b. d.	b. d.	6.84	6.84
Co	37.3	25.5	57.5	27.0	25.3	38.2	36.7	22.6	36.1	29.9	33.6	38.2	52.5	35.7	48.3	42.4	39.2	60.7	43.6	45.4
V	b. d.	b. d.	10	b. d.	b. d.	5	b. d	b. d	b. d	5	75	88	92	110	128	126	128	130	129	123
Cu	0.8	3.0	7.8	1.0	1.0	1.4	1.6	1.3	1.2	1.0	17.1	18.7	19.4	18.6	15.3	18.0	19.3	19.7	19.9	25.4
Pb	3.8	4.2	3.9	2.2	3.4	3.3	3.0	3.7	3.1	2.3	2.1	2.9	2.3	2.5	2.5	2.6	1.9	5.5	2.7	3.2
Zn	15	14	34	38	27	0.8	31	32	29	39	30	35	36	28	30	25	27	26	26	24
W	229.2	179.2	404.8	164.9	158.1	241.7	240.4	87.5	248.7	223.8	153.4	184.2	254.3	105.9	144.6	143.4	87.0	267.3	177.0	175.7
Rb	180.4	181.8	175.9	153.1	155.8	146.1	155.1	149.6	159.0	152.4	94.7	82.2	72.7	61.4	37.3	46.3	49.4	48.7	47.9	51.5
Cs	8.7	7.0	8.0	4.4	4.1	4.3	4.7	3.1	5.3	5.0	3.4	4.0	3.4	3.1	2.2	3.0	2.0	3.2	21.3	4.5
Ba	840	849	614	661	674	668	698	690	660	649	405	392	380	349	338	286	303	301	282	394
Sr	165.8	178.0	230.8	232.8	219.1	229.2	224.2	207.8	237.2	248.6	378.8	458.1	459.2	498.4	526.7	577.3	515.7	581.0	1095.6	482.5
Ga	20.8	21.5	22.9	17.9	19.5	18.7	21.1	20.5	20.7	20.9	21.6	24.2	20.8	24.5	23.2	21.2	23.5	23.1	22.8	21.9
Ta	1.1	1.1	1.0	1.1	1.1	1.0	1.1	1.0	1.3	1.2	0.9	0.9	1.2	1.1	1.1	0.9	1.0	1.0	1.1	1.5
Nb	9.8	9.9	9.2	9.0	8.9	8.6	8.8	9.6	9.6	9.2	9.4	10.7	10.6	12.9	13.9	12.6	12.8	12.7	12.8	12.9
Hf	2.3	2.5	3.6	3.8	2.8	3.4	3.5	3.0	3.5	3.3	5.2	4.7	4.5	4.0	4.7	4.0	4.6	4.3	4.4	4.4
Zr	54.2	53.8	131.8	107.3	93.4	111.3	100.8	102.4	113.3	126.0	206.6	187.7	180.4	169.3	202.8	171.4	178.6	180.5	174.7	177.4
Y	12.2	12.1	12.1	10.7	11.3	11.0	10.6	10.3	11.4	10.8	17.3	17.7	17.5	21.6	23.8	21.9	21.5	22.5	23.1	22.0
Th	14.3	16.2	22.2	21.4	22.6	21.3	22.6	25.1	25.1	23.9	12.4	10.1	9.6	9.1	7.1	6.5	6.7	6.0	6.5	6.6
U	5.6	4.5	5.1	4.6	4.7	4.3	3.6	5.5	5.4	5.5	2.9	4.2	3.3	2.1	3.1	1.8	2.4	1.9	2.2	1.8
La	22.3	22.7	42.3	42.9	45.2	42.5	46.3	43.8	44.8	42.0	27.3	26.7	26.2	23.7	23.8	21.1	22.0	21.4	20.8	22.7
Ce	42.5	43.9	76.1	74.3	78.6	75.4	82.2	77.1	77.4	74.3	51.6	49.9	49.7	44.5	46.2	43.3	44.1	43.7	42.5	44.1
Pr	4.46	4.82	7.81	7.85	8.21	7.81	8.38	8.11	8.24	7.39	6.07	5.89	5.77	5.38	5.77	4.86	5.24	5.18	5.08	5.04
Nd	16.0	16.8	27.8	26.4	27.2	26.3	28.1	28.1	27.3	26.2	23.5	24.6	21.7	22.5	25.1	21.7	23.1	22.2	22.3	22.5
Sm	3.3	3.3	4.6	3.6	4.5	4.2	4.2	4.7	4.2	4.3	5.5	4.9	4.9	4.2	5.4	4.7	5.0	5.4	4.4	5.2
Eu	0.54	0.70	0.84	0.78	0.85	0.84	0.91	0.81	0.90	1.03	1.25	1.48	1.35	1.37	1.54	1.40	1.59	1.46	1.52	1.49
Gd	2.50	2.16	2.73	2.82	2.28	2.42	2.89	2.60	3.16	2.71	3.63	4.02	4.37	4.40	4.21	4.20	4.43	4.48	4.47	4.34
Tb	0.38	0.38	0.42	0.35	0.38	0.40	0.38	0.37	0.35	0.39	0.60	0.62	0.62	0.65	0.69	0.75	0.71	0.70	0.76	0.68
Dy	1.84	1.77	2.01	1.66	2.17	1.70	1.84	1.75	1.95	1.86	3.13	3.40	3.25	3.86	4.27	3.68	4.06	3.87	4.12	4.20
Ho	0.34	0.38	0.42	0.33	0.34	0.33	0.34	0.35	0.33	0.36	0.57	0.64	0.60	0.73	0.86	0.75	0.73	0.74	0.80	0.76
Er	0.99	0.99	0.97	0.92	0.99	0.90	0.93	0.95	0.97	0.91	1.58	1.73	1.69	0.28	2.24	2.26	1.96	2.13	2.36	2.16
Tm	0.16	0.14	0.18	0.17	0.14	0.14	0.13	0.15	0.16	0.13	0.24	0.28	0.28	0.30	0.35	0.32	0.30	0.33	0.32	0.30
Yb	0.86	0.96	0.99	0.94	0.93	0.90	0.98	0.88	0.98	0.92	1.57	1.73	1.45	1.89	2.02	2.06	1.95	1.96	2.06	2.08
Lu	0.13	0.10	0.14	0.15	0.15	0.14	0.13	0.10	0.16	0.15	0.23	0.23	0.21	0.23	0.29	0.27	0.31	0.32	0.29	0.32
A. S. I	1.10	1.14	1.04	1.09	1.11	1.09	1.09	1.15	1.09	1.07	0.92	0.90	0.89	0.86	0.87	0.86	0.86	0.85	0.85	0.86
Mg #	12.73	18.35	23.72	16.48	17.18	14.53	13.25	25.54	15.11	14.04	31.75	32.17	33.75	32.58	30.49	33.54	32.28	32.75	33.97	33.12
Eu /Eu*	0.57	0.80	0.72	0.75	0.81	0.81	0.80	0.71	0.76	0.92	0.86	1.02	0.89	0.97	0.99	0.96	1.03	0.91	1.05	0.96
(La/Lu)CN	18	24	32	31	32	33	38	47	30	30	13	12	13	11	9	8	8	7	8	8

b.d.– blow detection, tFe_2O_3 represents total iron oxide as ferric iron, LOI– loss on ignition, OV-14* sample is a basaltic trachyandesite enclave found within the trachyandesite; Mg#= 100 x Mg / (Mg + tFe^{+2}); A. S. I. (A/CNK)= $(Al_2O_{3sample}/(Al_2O_3^*)$ / $[(CaO_{sample}/CaO^*) + (Na_2O_{sample}/Na_2O^*) + (K_2O_{sample}/K_2O^*)]$, * molecular weight of oxide component; Eu / Eu* = (Eu_{sample}/Eu_{CN}) / $[(Sm_{sample}/Sm_{CN})^*(Gd_{sample}/Gd_{CN})]^{1/2}$ (Taylor & McLenan 1985); $(La/Lu_{CN}) = (La_{sample}/La_{CN})$ / (Lu_{sample}/Lu_{CN}), (CN values from Sun & McDonough 1989).

Similar considerations about the Late Oligocene to Middle Miocene felsic volcanism in the western part of the southeastern Anatolian orogen have been recently reported by H. Yılmaz *et al.* (2007). They point out that elevated Rb/Sr ratios, low MgO and Fe_2O_3 total in the first stage of felsic volcanism suggest that the magma might represent melts lacking entrained Fe-Mg-rich crystals, and developed by muscovite-dehydration melting of the muscovite-bearing crustal metamorphic rocks of the Bitlis-Pötürge Massif following Late Oligocene–Early Miocene imbricate crustal thickening (H. Yılmaz *et al.* 2007). They proposed that the second felsic volcanism was generated by continental exhumation and lithospheric fracturing caused partial fusion of the mantle beneath the Anatolian crust during the Middle Miocene (H. Yılmaz *et al.* 2007). H. Yılmaz *et al.* (2007) also suggested that emplacement of hot, mantle-derived mafic melts in Anatolian lower crustal levels caused partial melting of lower crustal rocks to yield Middle Miocene felsic magmas. Therefore, a lower crustal origin of rhyolites and rhyolitic dykes from the Orduzu volcanics seems to be consistent with the hypothesis of H. Yılmaz *et al.* (2007), since they are spatially and temporally connected with the Middle Miocene felsic volcanism of the western part of the southeastern Anatolian orogen.

Andesitic and Basaltic-Trachyandesitic Rocks

Stratigraphical, textural, petrographical and geochemical data show that the andesitic and basaltic trachyandesitic dikes of the Orduzu volcanics were derived from two different, but coeval, mafic melts. The first melt is calc-alkaline (i.e. the trachyandesite) and the second one is mildly alkaline in composition (i.e. the basaltic trachyandesitic dykes). Prim-normalized spider diagrams of these two mafic melts are remarkably similar to one another, although the LREE contents of the trachyandesites are higher than those in basaltic trachyandesitic dykes, while the opposite is true of the HREE.

The magmatic source of these mafic magmas in the Orduzu volcanics seems to be an enriched mantle, metasomatized by subduction-derived fluids above an intra-oceanic subduction zone within the Neo-Tethyan oceanic realm. This enriched mantle source seems to be lithospheric rather than asthenospheric, as, using the La/Nb ratio indications (De Paolo & Daley 2000) the La/Nb ratios of both trachyandesites and basaltic trachyandesitic dykes exceed 1.0. Evidence for this is provided by the Prim-normalized trace, and Chondrite-normalized REE spider diagrams (Figure 9), as well as the Nb/Y versus Rb/Y variation diagram (Figure 10a). The source enrichment can be examined further using the Ta/Yb- Th/Yb diagram, which may be effectively used to display subduction-induced source metasomatism and crustal contamination (Pearce *et al.* 1990). The Nb/Y-Th/Y diagram shows that the trachyandesite and basaltic trachyandesitic dykes have lower Th/Nb ratios than those of the rhyolite and rhyolitic dykes (Figure 10b). The Th/Nb ratios of the trachyandesite are higher than those of the basaltic trachyandesitic dykes. This relative Th enrichment in the trachyandesite can result from fractional crystallization combined with crustal contamination. On the other hand, both the mafic and felsic rocks plot outside the mantle array due mainly to higher Th/Yb ratios (Figure 10c). Such higher ratios may suggest derivation from an enriched mantle source into which a subduction component was added. This conclusion agrees with the REE and trace-element data reported by Önal *et al.* (2004). Additionally, crustal contribution to the magma source of the trachyandesite is also suggested by proximity of the rock samples from this unit to the average upper crust along the fractional crystallization trend (Figure 10c).

In the light of all these comparisons, it can be suggested that the magma source of the trachyandesite could have been generated by the partial melting of an enriched lithospheric mantle. Basaltic trachyandesitic dykes, by contrast, were probably derived from another lithospheric mantle source which was probably garnet-free because it contained more HREE, and was probably derived by a low degree of partial melting because of its mildly alkaline composition.

Magma Mixing

Magma mingling and mixing events seem to have occurred between the coeval mafic magmas, i.e. the trachyandesite and basaltic trachyandesitic dykes rather than between basaltic and rhyolitic magmas in the genesis of the Orduzu volcanics. The unusual globular occurrences consisting of pyroxene and biotite microcrystals set in a feldspar-rich groundmass, and some plagioclase phenocrysts, showing oscillatory zoning

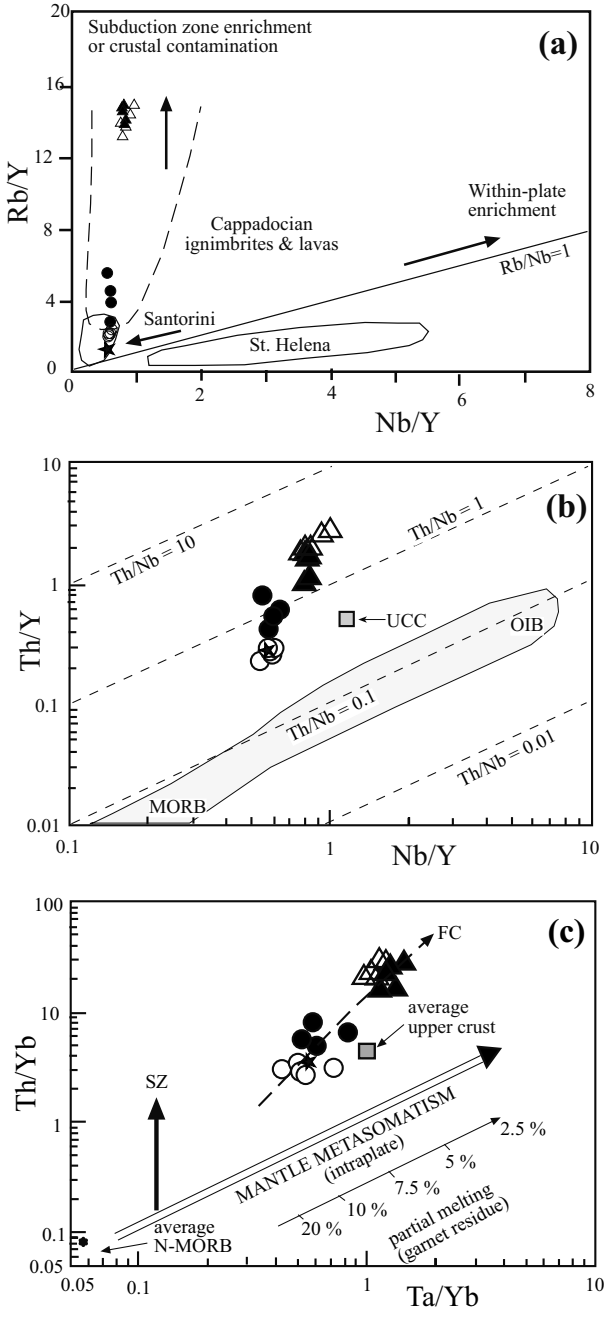

Figure 10. (a) Nb/Y-Rb/Y; (b) Nb/Y-Th/Y; (c) Ta/Yb-Th/Yb plots of the Orduzu volcanics (diagrams are taken from Temel *et al.* 1998; Tankut *et al.* 1998; Pearce *et al.* 1990, respectively). For legend see Figure 7.

with some mafic mineral inclusions regularly arranged along the crystal margins or randomly scattered, are considered to be the textural evidence of magma mixing (Tsuchiyama 1985; Gaurgaud 1991; Feeley & Dungan 1996; Screiber *et al.* 1999). In addition to these textures, the hyperbolic trend in HFSE and LILE ratio plots (Figure 11a, b) is regarded as the geochemical evidence for magma mixing, as suggested by Seymour & Vlassopoulos (1992).

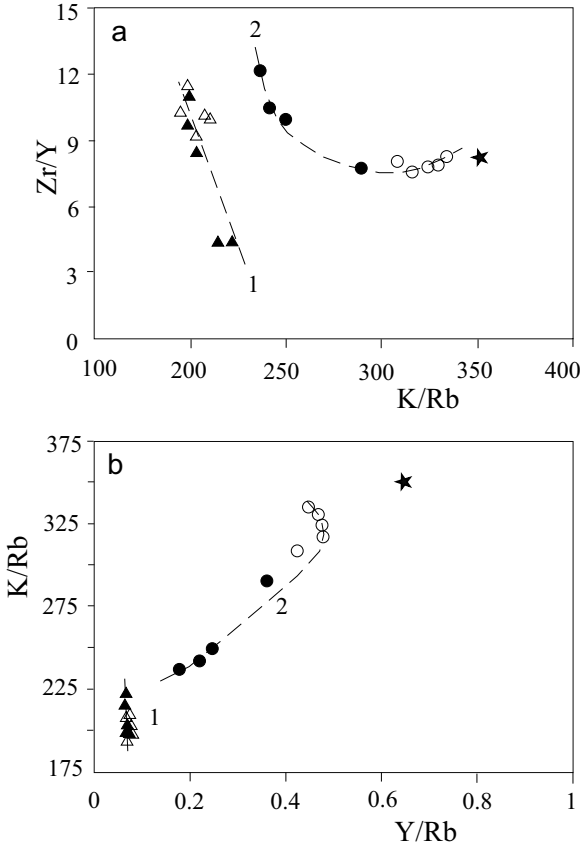

Figure 11. (a) K/Rb-Zr/Y; (b) Y/Rb-K/Rb plots of the Orduzu volcanics system. Hyperbolic distributions of trachyandesite and basaltic trachyandesitic dykes indicate mixing (diagrams are taken from Seymour & Vlassopoulos 1992). For legend see Figure 7.

Geodynamic Implications

As mentioned earlier, many previous studies have related the genesis of the Neogene volcanism in eastern Anatolia to the Late Cenozoic convergence of the African-Arabian system with Anatolia which led to Oligo–Miocene collision and a strong N–S compression in eastern Anatolia. This investigation of the Orduzu volcanics brings two major contribution into the geological evolution of the eastern Anatolian volcanism: firstly the Middle Miocene age revealed by ^{40}Ar-^{39}Ar age determination carried out on the plagioclase separates, and secondly the enriched mantle source rocks, giving a subduction signature.

The Middle Miocene seems to be consistent with a post-collisional setting of the Orduzu volcanics. Various workers have proposed that the collision between Africa-Arabia system and Anatolia occurred in the Middle Eocene (Hempton 1985), or the Middle Eocene to Miocene (Yılmaz 1993; H. Yılmaz *et al*. 1993) or during the Oligocene to Miocene (Elmas & Yılmaz 2003) in eastern Anatolia. However, the post-collisional related geodynamic setting of the Middle Miocene felsic volcanism in the Malatya region was also emphasized by H. Yılmaz *et al.* (2007) and related to the collision system between the Eurasian and Arabian plates.

We propose that the subduction signature in the enriched mantle source was derived from mantle metasomatism caused by the introduction of fluids sourced from an earlier supra-subduction zone. Such subduction-derived fluids can affect the overlying mantle wedge above a subduction zone, yielding an enriched mantle layer carrying a subduction signature (e.g., Pearce *et al.* 1990). Accreted, already metasomatized mantle slices in the collision zone may melt later in a post-collisional setting giving rise to produce the mantle-derived magma sources of the Orduzu volcanics in the Malatya region in eastern Anatolia, which are comparable to post-collisional volcanics previously reported from various parts of eastern Anatolia (Ercan *et al*. 1990; Pearce *et al*. 1990; Yılmaz 1990; Keskin *et al*. 1998; Yalçın *et al*. 1998; Arger *et al*. 2000; Kürüm *et al*. 2004).

Conclusion

The ^{40}Ar-^{39}Ar geochronological, petrographic, and whole-rock and mineral chemical data reported here suggest that three different coeval magmas (i.e. rhyolitic, andesitic and basaltic trachyandesitic) were involved in the genesis of the felsic and mafic rocks of the Orduzu volcanics. Mingling and mixing between andesitic and basaltic trachyandesitic melts is especially evident from both textures and compositions in the trachyandesite and basaltic trachyandesitic dykes. Trace-element and REE data indicate that, in addition to crustal contamination, there is also a conspicuous subduction signature in the mantle-derived volcanic rocks of the Orduzu volcanic system.

Acknowledgement

This study has been partially supported by a grant (BAP 2001/26) from the Scientific Resarch Project of the İnönü University. Authors thank to Sergei MATVEEV for performing EPMA. We thank Gültekin Topuz and an anonymous reviewer for their helpful comments which substantially improved the manuscript. Erdin Bozkurt is kindly thanked for his editorial work. John A. Winchester edited the English of the final text.

References

ALPASLAN, M., YILMAZ, H. & TEMEL, A. 2004. Geochemistry of post-collision Pliocene–Quaternary Karaşar basalt (Divrigi-Sivas, Eastern Turkey): Evidence for partial melting processes. *Geologica Carpathica* **55**, 487–500.

ARGER, J., MITCHEL, J. & WESTAWAY, R.W.C. 2000. Neogene and Quaternary volcanism of southeastern Turkey. *In*: BOZKURT, E., WINCHESTER, J.A. & PIPER, J.D.A. (eds), *Tectonics and Magmatism in Turkey and its Surrounding Area*. Geological Society, London, Special Publications **173**, 459–487.

ARMSTRONG, J.T. 1995. A package of correction programs for the quantitative electron microbeam X-ray analysis of thick polished materials, thin films, and particles. *Microbeam Analysis* **4**, 177–200.

BRIGATTI, M.F., MEDICI, L., SACCANI, E. & VACCARO, C. 1996. Crystal chemistry and petrologic significance of Fe (super 3+)-rich phlogopite from the Tapira carbonatite complex, Brazil. *American Mineralogist* 81, 913–927.

CEBULA, G.T., KUNK, M.J., MEHNERT, H.H., NAESER, C.W., OBRADOVICH, J.D. & SUTTER, J.F. 1986. The Fish Canyon Tuff, a potential standard for the ^{40}Ar-^{39}Ar and fission-track dating methods. *In*: 6th International Conferance on Geochronology, *Cosmochronology and Isotope Geology* 6, Terra Cognita, p. 139.

DEMİR, O. 1997. *Malatya, İsmetpaşa, Akçadağ, Kürecik, Hekimhan, Arguvan ve Karakaya Baraj Gölü Arasındaki Alanın Jeolojisi ve Hidrokarbon Olanakları [Geology and Hydrocarbon Potential of the Area Between Malatya, İsmetpaşa, Akçadağ, Kürecik, Hekimhan, Arguvan and Karakaya Dam*]. Turkish Petroleum Corporation Report no. **3781**[in Turkish, unpublished].

DE PAOLO, D.J. & DALEY, E.E. 2000. Neodymium isotopes in basalts of the southwest basin and range and lithospheric thinning during continental extension. *Chemical Geology* **169**, 157–185.

ELMAS, A. & YILMAZ, Y. 2003. Development of an oblique subduction zone – Tectonic evolution of the Thethys suture zone in southeast Turkey. *International Geology Review* **45**, 827–840.

EKİCİ, T., ALPASLAN, M., PARLAK, O. & TEMEL, A. 2006. Geochemistry of the Pliocene basalts erupted along the Malatya-Ovacık fault zone (MOFZ), eastern Anatolia, Turkey: Implications for source characteristics and partial melting processes. *Chemie der Erde Geochemistry* **67**, 201–212..

ERCAN, T., FUJITANI, T., MATSUDA, J.I., TOKEL, S., NOTSU, K., UI, T., CAN, B., SELVİ, Y., YILDIRIM, T., FİŞEKÇİ, A., ÖLMEZ, M. & AKBAŞLI, A. 1990. The origin and evolution of the Cenozoic volcanism of Hasandağı-Karacalıdağ area (Central Anatolia). *Bulletin of Geomorphology* **18**, 9–54.

FARMER, G.L. & BOETTCHER, A.L. 1981. Petrologic and crystal-chemical significance of some deep-seated phlogopites. *American Mineralogist* **66**, 1154–1163.

FEELEY, T.C. & DUNGAN, M.A. 1996. Compositional and dynamic controls on mafic-silicic magma interactions at continental arc volcanoes: evidence from Cordon El Guadal, Tatara–San Pablo Complex, Chile. *Journal of Petrology* **37**, 1547–1577.

GAURGAUD, A. 1991. Comagmatic enclaves in lavas from the Mont-Dore composite volcano, Massif Central, France. *In*: DIDIER, J. & BARBARIN, B. (eds), *Enclaves and Granite Petrology* . Developments in Petrology **13**, Elsevier, 221–233.

HEMPTON, M.R. 1985. Structure and deformation history of the Bitlis suture near Lake Hazar, southeastern Turkey. *Geological Society of America Bulletin* **96**, 233–243.

HIBBARD, M.J. 1991. Textural anatomy of twelve magma-mixed granitoid systems. *In*: DIDIER, J. & BARBARIN, B. (eds), *Enclaves and Granite Petrology* . Developments in Petrology **13**, Elsevier, 431–444.

INNOCENTI, F., MANETTI, P., MAZZUOLI, R., PASQUARE, G. & VILLARI, L. 1982. Anatolia and northwestern Iran. *In*: THORPE, R.S. (ed), *Andesites*. Wiley, 327–349.

IRVINE, T.N. & BARAGAR, W.R.A. 1971. A guide to the chemical classification of common volcanic rocks. *Canadian Journal of Earth Sciences* **8**, 523–548.

JAROSEWICH, E. 2002. Smithsonian microbeam standards. *Journal of Research of the National Institute of Standards and Technology* **107**, 681–685.

KESKİN, M. 2003. Magma generation by slab steepening and break-off beneath a subduction-accretion complex: an alternative model for collision-related volcanism in eastern Anatolia, Turkey. *Geophysical Research Letters* **30**, 8046, doi: 10.1029/2003 GL018019, 2003.

KESKİN, M., PEARCE, J.A. & MITCHEL, J.G. 1998. Volcano-stratigraphy and geochemistry of collision volcanism on the Erzurum-Kars plateau, northeastern Turkey. *Journal of Volcanology and Geothermal Research* **85**, 355–404.

KESKİN, M., PEARCE, J.A., KEMPTON, P.D. & GREENWOOD, P. 2006. Magma-crust interactions and magma plumbing in a postcollisional setting: Geochemical evidence from the Erzurum-Kars volcanic plateau, eastern Turkey. *In*: DİLEK, Y. & PAVLIDES, S (eds), *Postcollisional Tectonics and Magmatism in the Mediterranean Region and Asia*. Geological Society of America, Special Paper **409**, 475–505.

KOYAGUCHI, T. 1991. Enclaves in volcanic rocks from Japan. *In*: DIDIER, J. & BARBARIN, B. (eds), *Enclaves and Granite Petrology* Developments in Petrology **13**, Elsevier, 235–250.

KÜRÜM, S., ÖNAL, A., BOZTUĞ, D., ARSLAN, M. & SPELL, T. 2004. $^{40}Ar/^{39}Ar$ age determination and geochemistry of the widespread Yamadağ volcanics in the Arapkir, N Malatya region, Eastern Anatolia, Turkey. *In*: CHATZIPETROS, A.A. & PAVLIDES, S.B. (eds), *Proceedings 5th International Symposium on Eastern Mediterranean Geology*, Thessaloniki, Greece, Abstracts, Volume **3**, 1295–1298.

LE BAS, M.J., LE MAITRE, R.W., STRECKEISEN, A. & ZANETTIN, B. 1986. A chemical classification of volcanic rocks based on the total alkali-silica diagram. *Journal of Petrology* **27**, 745–750.

LE MAITRE, R.W., BATEMAN, P., DUDEK, A., KELLER, J., LAMEYRE, J., LE BAS, M.J., SABINE, P.A., SCHMID, R., SORENSEN, H., STRECKEISEN, A., WOOLLEY, A.R. & ZANETTIN, B. 1989. *A Classification of Igneous Rocks and Glossary of Terms*. Recommendations of the IUGS Subcommission on the Systematics of Igneous Rocks, Blackwell Scientific Publication, Trowbridge, Wilts.

LEO, G.W., MARVIN, R.F. & MEHNERT, H.H. 1974. Geologic framework of the Kuluncak-Sofular area, east-central Turkey, and K-Ar ages of igneous rocks. *Geological Society of America Bulletin* **85**, 1785–1788.

MORIMOTO, M. 1988. Nomenclature of pyroxenes. *Mineralogical Magazine* **52**, 535–550.

ÖNAL, AY., BOZTUĞ, D., ARSLAN, M., SPELL, T., KÜRÜM, S. & ÖNAL, A. 2004. Geochemistry and $^{40}Ar/^{39}Ar$ geochronology of the felsic and mafic lava flows in the Orduzu (Malatya) volcanic cone from the widespread Neogene Yamadağ volcanism, Eastern Anatolia, Turkey. *In*: CHATZIPETROS, A.A. & PAVLIDES, S.B. (eds), *Proceedings 5th International Symposium on Eastern Mediterranean Geology*, Thessaloniki, Greece, Abstracts, Volume **3**, 1302–1305.

ÖZDEMİR, Y., KARAOĞLU, Ö., TOLLUOĞLU, A.Ü. & GÜLEÇ, N. 2006. Volcanostratigraphy and petrogenesis of the Nemrut stratovolcano (East Anatolian High Plateau): The most recent post-collisional volcanism in Turkey. *Chemical Geology* **226**, 189–211.

PEARCE, J.A., BENDER, J.F., DE LONG, S.E., KIDD, W.S.F., LOW, P.J., GÜNER, Y., ŞAROĞLU, F., YILMAZ, Y., MOORBATH, S. & MITCHEL, J.G. 1990. Genesis of collision volcanism in eastern Anatolia, Turkey. *Journal of Volcanology and Geothermal Research* **44**, 189–229.

SCREIBER, U., ANDERS, D. & KOPPEN, J. 1999. Mixing and chemical interdiffusion of trachytic and latitic magma in a subvolcanic complex of the Tertiary Westerwald (Germany). *Lithos* **46**, 695–714.

ŞENGÖR, A.M.C., ÖZEREN, S., GENÇ, T. & ZOR, E. 2003. East Anatolian high plateau as a mantle-supported, north–south shortened domal structure. *Geophysical Research Letters* **30**, 8045, doi: 10.1029/2003GL017858.

SEYMOUR, K.S.T. & VLASSOPOULOS, D. 1992. Magma mixing at Nisyros volcano, as inferred from incompatible trace-element systematics. *Journal of Volcanology and Geothermal Research* **50**, 273–299.

STAUDACHER, T.H., JESSBERGER, E.K., DORFLINGER, D. & KIKO, J. 1978. A refined ultrahigh-vacuum furnace for rare gas analysis, *Journal of Physics Series E: Scientific Instruments* **11**, 781–784.

STEVEN, T.A., MEHNERT, H.H. & OBRADOVICH, J.D. 1967. Age of volcanic activity in the San Juan Mountains, Colorado. *United States Geological Survey Professional Paper* **575** (D), 47–55.

SUN, S.S. & MCDONOUGH, W.F. 1989. Chemical and isotopic systematics of oceanic basalts: implications for mantle composition and processes. *In:* SAUNDERS, A.D. & NORRY, M.J. (eds), *Magmatism in the Ocean Basins*. Geological Society, London, Special Publications **42**, 313–345.

TANKUT, A., WILSON, M. & YIHUNIE, T. 1998. Geochemistry and tectonic setting of Tertiary volcanism in the Güvem area, Anatolia, Turkey. *Journal of Volcanology and Geothermal Research* **85**, 285–301.

TAYLOR, S.R. & MCLENNAN, S.M. 1985. *The Continental Crust: Its Composition and Evolution*. Blackwell Scientific.

TEMEL, A., GÜNDOĞDU, M.N. & GAURGAUD, A. 1998. Petrological and geochemical characteristics of Cenozoic high-K calc-alkaline volcanism in Konya, Central Anatolia, Turkey. *Journal of Volcanology and Geothermal Research* **85**, 327–354.

TSUCHIYAMA, A. 1985. Dissolution kinetics of plagioclase in the melt of the system diopside-albite-anorthite and origin of dusty plagioclase in andesites. *Contributions to Mineralogy and Petrology* **89**, 1–16.

YALÇIN, H., GÜNDOĞDU, M.N., GOURGAUD, A., VIDAL, P. & UÇURUM, A. 1998. Geochemical characteristics of Yamadağı volcanics in central east Anatolia: an example from collision-zone volcanism. *Journal of Volcanology and Geothermal Research* **85**, 303–326.

YILMAZ, H., ALPASLAN, M. & TEMEL, A. 2007. Two-stage felsic volcanism in the western part of the southeastern Anatolian orogen: Petrologic and geodynamic implications. *International Geology Review* **49**, 120–141.

YILMAZ, S., BOZTUĞ, D. & ÖZTÜRK, A. 1993. Geological setting, petrographic and geochemical characteristics of the Cretaceous and Tertiary igneous rocks in the Hekimhan-Hasançelebi area, north-west Malatya, Turkey. *Geological Journal* **28**, 383–398.

YILMAZ, Y. 1990. Comparison of young volcanic associations of western and eastern Anatolia formed under a compressional regime: a review. *Journal of Volcanology and Geothermal Research* **44**, 69–87.

YILMAZ, Y. 1993. New evidence and model on the evolution of the southeast Anatolian orogen. *Geological Society of America Bulletin* **105**, 251–271.

YILMAZ, Y. YİĞİTBAŞ, E. & GENÇ, Ş.C. 1993. Ophiolitic and metamorphic assemblages of southeast Anatolia and their significance in the geological evolution of the orogenic belt. *Tectonics* **12**, 1280–1297.

Received 14 November 2006; revised typescript received 25 May 2007; accepted 09 October 2007